THE ASTROPHYSICAL JOURNAL, 458:73–99, 1996 February 10

TWO-POINT VELOCITY AND SPATIAL CORRELATION FUNCTIONS OF THE C IV ABSORPTION SYSTEMS TOWARD THE TOLOLO QUASAR GROUP: EVIDENCE FOR SUPERCLUSTERING AT $z \simeq 2$[1]

NADINE DINSHAW AND CHRIS D. IMPEY
Steward Observatory, University of Arizona, Tucson, AZ 85721
Received 1995 May 16; accepted 1995 August 11

ABSTRACT

The large number of apparently correlated C IV absorption systems observed in the lines of sight to the wide QSO pair Tol 1037−2704 ($z_{em} = 2.193$) and Tol 1038−2712 ($z_{em} = 2.331$) between the redshifts $1.88 \leq z \leq 2.15$ is thought to be produced by an intervening supercluster. We present high-resolution echelle spectra of Tol 1037−2704 and Tol 1038−2712, as well as two neighboring QSOs with the aim of searching for absorption associated with the putative supercluster. The lines of sight toward the original pair are separated by 17'.9 corresponding to a proper separation of $D_\perp \simeq 4.4\ h^{-1}$ Mpc ($h = H_0/100$ km s^{-1} Mpc^{-1}; $q_0 = 0.5$) at $z = 2$. We confirm the existence of the C IV absorption complexes already reported, and find additional complexes. At a resolution of ~ 30 km s^{-1} FWHM, many of the C IV complexes break up into multiple discrete components with a velocity spread of $\Delta v \simeq 50$–1000 km s^{-1}. This brings the total number of C IV absorption systems with secure identifications to 22 in Tol 1037−2704 and 11 in Tol 1038−2712 in the redshift range $1.48 \leq z \leq 2.15$, well above the expectation from Poisson statistics. The two neighboring QSOs, Tol 1035−2737 ($z_{em} = 2.159$) and Tol 1029−2654 ($z_{em} = 2.586$), are located roughly 40' ($D_\perp \simeq 10\ h^{-1}$ Mpc) southwest and 115' ($D_\perp \simeq 30\ h^{-1}$ Mpc) northwest of the Tololo pair, respectively. We found five C IV systems in the line of sight to Tol 1035−2737, and six toward Tol 1029−2654. Most of these systems appear to match systems in the original QSO pair within a velocity separation of less than 5000 km s^{-1}, though the significance of the matches is not strong. We find a marginal excess of C IV absorption systems in the line of sight to Tol 1029−2654, whereas the number of systems in the line of sight to Tol 1035−2737 agrees with expectation. The inferred proper dimensions of the proposed supercluster are at least $30\ h^{-1}$ Mpc on the plane of the sky and approximately $80\ h^{-1}$ Mpc along the line of sight.

We examined the clustering properties of the absorbers toward the Tololo QSOs using the two-point velocity and spatial correlation functions. The velocity correlation function of the complete sample of 44 C IV systems shows strong clustering for velocity separations less than 1000 km s^{-1}, which probe clouds in galactic halos as well as individual galaxies in clusters, and significant clustering signal out to scales of 7000 km s^{-1}. In a subsample of 16 systems ($W_0 > 0.15$ Å), where the power associated with virialized clusters on scales less than 1000 km s^{-1} has been removed, significant correlation signal persists for velocity separations of 4000–7000 km s^{-1}, which correspond to comoving spatial scales of ~ 30–$40\ h^{-1}$ Mpc. The spatial correlation function of the same subsample, derived by pairing absorbers between different lines of sight, shows a marginally significant peak on comoving scales of less than 18 Mpc. The clustering amplitude on these scales is larger than predicted by current theories of the formation of large-scale structure.

Subject headings: galaxies: clusters: general — quasars: general — quasars: absorption lines

1. INTRODUCTION

The absorption lines of heavy elements observed in the spectra of QSOs are powerful probes of large-scale structure at high redshift. Since they appear to cluster in velocity space with an amplitude and scale similar to that expected from galaxy clustering (Sargent, Boksenberg, & Steidel 1988, hereafter SBS), the absorbers responsible for the heavy element absorption lines are thought to be associated with galaxies or their precursors. Direct evidence for this association comes from recent identifications of the galaxies associated with the Mg II absorption (Bergeron & Boisse 1991; Steidel 1993). By analogy with the Mg II results, the C IV absorption systems, which are observable from the ground for redshifts $1.2 \lesssim z \lesssim 4$, are thought to define a sample of normal galaxies and provide the only means of studying these galaxies at high redshift, since optical identifications at $z > 1$ are not yet feasible.

Recent evidence indicates very large-scale superclustering of the C IV absorbers. Heisler, Hogan, & White (1989, hereafter HHW) found significant clustering signal out to velocities of $\Delta v = 10{,}000$ km s^{-1} in a large sample of C IV systems detected toward 55 QSOs. The signal is dominated by a single large supercluster along the line of sight to the QSO PKS 0237−233, which shows a large (≥ 20) overdensity of C IV absorbers at $z \simeq 1.65$. In a follow up survey for nearby QSOs to be used as background probes, Foltz et al. (1993) found an overdensity of C IV systems in the redshift range $1.57 \lesssim z \lesssim 1.69$ along the lines of sight to six QSOs, with most of the absorption seen toward two QSOs. Similarly, Francis & Hewett (1995) discovered two damped Lyα absorption systems at similar redshifts in the spectra of two high-redshift QSOs ($z \simeq 3.2$) separated by a comoving distance of $\sim 18\ h^{-1}$ Mpc. Since high column density hydrogen absorbers are believed to

[1] Observations reported here were obtained with the Cerro Tololo Inter-American Observatory 4 m Telescope, which is operated by the Association of Universities for Research in Astronomy, Inc., under contract from the National Science Foundation

be associated with the disks of spiral galaxies, this result suggests the presence of a large coherent structure at $z > 2$. Recent pencil-beam surveys suggest that galaxies cluster on very large scales with an apparent periodicity in their distribution on a characteristic scale of 128 h^{-1} Mpc (Broadhurst et al. 1990), although the significance of the results has been disputed (Kaiser & Peacock 1991).

Another important example of superclustered absorption is observed along the lines of sight to the wide QSO pair Tol 1037−2704 ($z_{em} = 2.193$) and Tol 1038−2712 ($z_{em} = 2.331$), whose spectra exhibit a number of apparently correlated C IV absorption systems (Jakobsen et al. 1986, hereafter J86; Sargent & Steidel 1987, hereafter S87). The spectra of the QSOs each exhibit at least five C IV complexes over the narrow redshift range $1.88 \lesssim z \lesssim 2.15$, representing a highly significant overdensity in the number of absorbers above that expected from Poisson statistics. One complex lies at the same redshift in both QSOs and the rest are coincident to within $v \leq 2000$ km s^{-1}. The QSOs have an angular separation of 17.9, corresponding to a proper separation on the sky of 4.4 h^{-1} Mpc.

The favored hypothesis for the overdensity of C IV absorption systems is that the two lines of sight intersect material associated with an intervening supercluster (J86; S87). The matter is arranged in a filamentary or sheetlike structure with proper dimensions of $\sim$50 Mpc along the line of sight and $\sim$10 Mpc in the plane of the sky, with the implication that we are viewing it from a special direction along the filament (S87; Jakobsen & Perryman 1992, hereafter J92). Such dimensions are consistent with the sizes of superclusters observed in the local universe. Many of the absorption complexes are split into narrower components spanning the velocity range $\Delta v \simeq 50$–1000 km s^{-1}. Velocity separations greater than 300 km s^{-1} are probably not due to cloud motions within galaxies but are consistent with the hypothesis that some of the components arise from the halos of individual galaxies in a cluster (S87). In this scenario, the more complex systems arise from the denser central region of a cluster and the single component systems are produced in the less dense outer region.

Although a plausible picture of the absorption being due to an intervening supercluster is emerging, this interpretation is not universally accepted (Christiani, Danziger, & Shaver 1987; Robertson 1987). The supercluster hypothesis is complicated by the fact that both Tol 1037−2704 and Tol 1038−2712 display broad absorption line (BAL) characteristics, which are generally thought to have an intrinsic origin, e.g., ejection or outflow of material from the QSO (Weymann, Carswell, & Smith 1981). S87 have presented physical arguments against ejection based on the energetics required to accelerate material to such great distances that it would be seen along both lines of sight, as well as statistical objections to the hypothesis that the lines could be due to independent ejections from both QSOs.

One recent line of study has been to locate other QSOs in the field surrounding the pair that are bright enough and at high enough redshifts to use as background probes of the hypothetical supercluster (S87; Jakobsen, Perryman & Christiani 1988, hereafter J88; J92). So far, this approach has met with modest success. One nearby QSO, Tol 1038−2707 ($z_{em} = 1.937$), which is 5′ from Tol 1038−2712, shows a strong absorption system with redshift close to the C IV system near $z_{abs} = 1.90$ in both Tol 1037−2704 and Tol 1038−2712 (J88). Another more promising candidate Tol 1035−2737 ($z_{em} = 2.159$) shows matches at $z_{abs} = 1.982$ and 2.125 (S87; J88).

The existence of a supercluster at these redshifts causes problems for the standard cold dark matter (CDM) model for structure formation, since structures on supercluster scales are not expected to form until redshifts closer to unity (Evrard, Summers, & Davies 1994). The theoretical implications of the proposed supercluster toward the Tololo QSO pair makes further research on the pair and surrounding QSOs particularly relevant, since the nature of the superclustering is not only of interest for investigations of the absorption clouds, but also for understanding the formation and evolution of large-scale structure at high redshift.

In this paper, we present high-resolution echelle spectra of the original Tololo pair and two neighboring QSOs within a 2°.5 × 1°.5 field, with the aim of searching for absorption associated with the proposed supercluster. The observations and reductions are described in § 2, and the technique used to identify the lines is described in § 3. In § 4, we discuss the QSOs and their absorption lines, and in § 5 we investigate the properties of the C IV systems. In § 6, we present and interpret the two-point redshift and spatial correlation functions of the C IV absorption systems. Finally, in § 7 we discuss the results in the context of the intervening supercluster hypothesis. Throughout this paper, we assume $H_0 = 100$ km s^{-1} Mpc^{-1} and $q_0 = 0.5$.

2. OBSERVATIONS AND REDUCTIONS

We obtained high-resolution spectroscopy of the QSOs listed in Table 1 during the period 1992 February 29 to March 3 UT using the Echelle Spectrograph and Air Schmidt camera on the 4 m telescope of the Cerro Tololo Inter-American Observatory. We used the 79 lines mm^{-1} echelle grating and KPGL2 cross disperser with the Reticon CCD to give a wavelength coverage from 3810–5130 Å in 15 echelle orders. The observations were made using a 1″.5 slit, which projected onto about 2.2 detector pixels. This gave a spectral resolution of

TABLE 1

PROGRAM QUASARS

QSO	R.A. (1950)	Decl. (1950)	m_B	z_{em}
Tol 1037–2704.....	$10^h36^m00^s.1$	−27°03′37″	17.4	2.193
Tol 1038–2712.....	10 38 10.4	−27 12 08	17.9	2.331
Tol 1035–2737.....	10 35 47.2	−27 37 14	19.0	2.159
Tol 1029–2654.....	10 29 35.4	−26 54 18	19.5	2.586

NOTE.—All coordinates, magnitudes, and redshifts are from Jakobsen & Perryman 1992, except for Tol 1029−2654, whose coordinates and magnitude were estimated from our objective prism survey. Details of the redshift determination for this object are given in the text.

TABLE 2

JOURNAL OF OBSERVATIONS

QSO	Date	Exposure (s)	Wavelength (Å)	Resolution (Å)
Tol 1037–2704.....	1992 Feb 29	5400	3810 – 5130	0.15
	1992 Feb 29	5400	3810 – 5130	0.15
	1992 Feb 29	5400	3810 – 5130	0.15
Tol 1038–2712.....	1992 Feb 29	5400	3810 – 5130	0.15
	1992 Feb 29	5400	3810 – 5130	0.15
	1992 Mar 1	5400	3810 – 5130	0.15
	1992 Mar 1	5400	3810 – 5130	0.15
Tol 1029–2654.....	1992 Mar 2	5400	3810 – 5130	0.15
	1992 Mar 2	5400	3810 – 5130	0.15
	1992 Mar 2	5400	3810 – 5130	0.15
	1992 Mar 2	5400	3810 – 5130	0.15
	1992 Mar 2	7200	3810 – 5130	0.15
Tol 1035–2737.....	1992 Mar 3	5400	3810 – 5130	0.15
	1992 Mar 3	5400	3810 – 5130	0.15
	1992 Mar 3	5400	3810 – 5130	0.15
	1992 Mar 3	5400	3810 – 5130	0.15
	1992 Mar 3	8400	3810 – 5130	0.15

$\sim$30 km s^{-1} FWHM, which varied slightly across the echelle orders, as measured from comparison arc lamp lines. The slit was aligned at the parallactic angle between each exposure to minimize light losses due to atmospheric refraction. The seeing was usually better than 1".5 FWHM. Exposure times of the QSO spectra were typically 5400 s up to a maximum of 8400 s. Table 1 lists the epoch 1950 coordinates, apparent blue magnitudes, and emission redshifts of the program QSOs, and Table 2 contains a log of the observations. The field in which the QSOs are located is shown in Figure 1.

We reduced the data in IRAF using tasks specifically designed for processing echelle spectra. Pixel-to-pixel variations in the detector response were normalized using a quartz lamp exposure. The orders were extracted using the optimal extraction technique of Horne (1986). At the same time, a variance array was determined for each spectrum from the object and sky background counts. Wavelength calibration was carried out using short exposures of a thorium-argon lamp, obtained before and after each object exposure. Bracketing comparison spectra were extracted using the same spatial weights as were used for the object spectrum. Standard errors in the wavelength calibration were not more than 0.018 Å.

The individual spectra were then rebinned onto a linear wavelength scale with pixels of 0.15 Å and co-added into a final spectrum for each QSO. A minmax rejection algorithm was used during the summation to eliminate the many cosmic-ray spikes, with some resulting reduction of S/N. The variance arrays of the individual spectra were similarly combined into a single array at this stage. The resulting spectra and their 1 σ error arrays are shown in Figures 2–5.

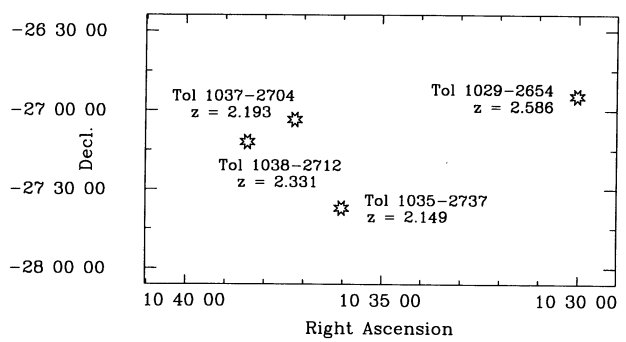

FIG. 1.—Field of Tol 1037–2704, Tol 1038–2712, Tol 1035–2737, and Tol 1029–2654. At $z = 2$, 10′ on the sky is 2.5 h^{-1} Mpc.

The QSO spectra were analyzed using software written by J. Bechtold and adapted by T. Aldcroft (see Bechtold 1994 for details). The continuum of each spectrum was estimated iteratively by fitting a cubic spline to regions that appeared free of absorption lines and the spectrum was normalized using this fit. Each pixel in the normalized spectrum was then evaluated for the presence of an absorption line by calculating the equivalent width and its uncertainty σ_W in a bin of width 2.5 × FWHM of the instrumental PSF centered on the pixel in question. This effectively excluded spurious features or noise spikes. The pixel was flagged if the equivalent width in the bin exceeded a threshold limit of $5\sigma_W$. Once all the significant lines were determined in this way, their equivalent widths were measured in an interactive manner by marking the beginning and ending wavelengths over which to carry out the summation. The line centers were determined over the same wavelength range using a centroiding algorithm, which weights each pixel by the depression with respect to the continuum. For weak lines ($< 10\sigma_W$ in strength), the central wavelengths were derived from Gaussian fits to the lines (see Young, Sargent, & Boksenberg 1982). The equivalent widths and vacuum wavelengths of all the lines are given in Tables 3, 4, 5, and 6. The wavelengths have been referenced to the heliocentric frame.

An attempt was made to separate the lines in complexes or blends by fitting multiple Gaussians only if it was deemed possible to get a good fit. The equivalent widths of these lines were derived from the Gaussian profiles and cannot be considered wholly reliable, especially in the broad complexes where the lines are not well represented by Gaussians. The line centers are nevertheless reliably determined, although their true uncertainties are probably larger than the quoted formal errors from the profile fits.

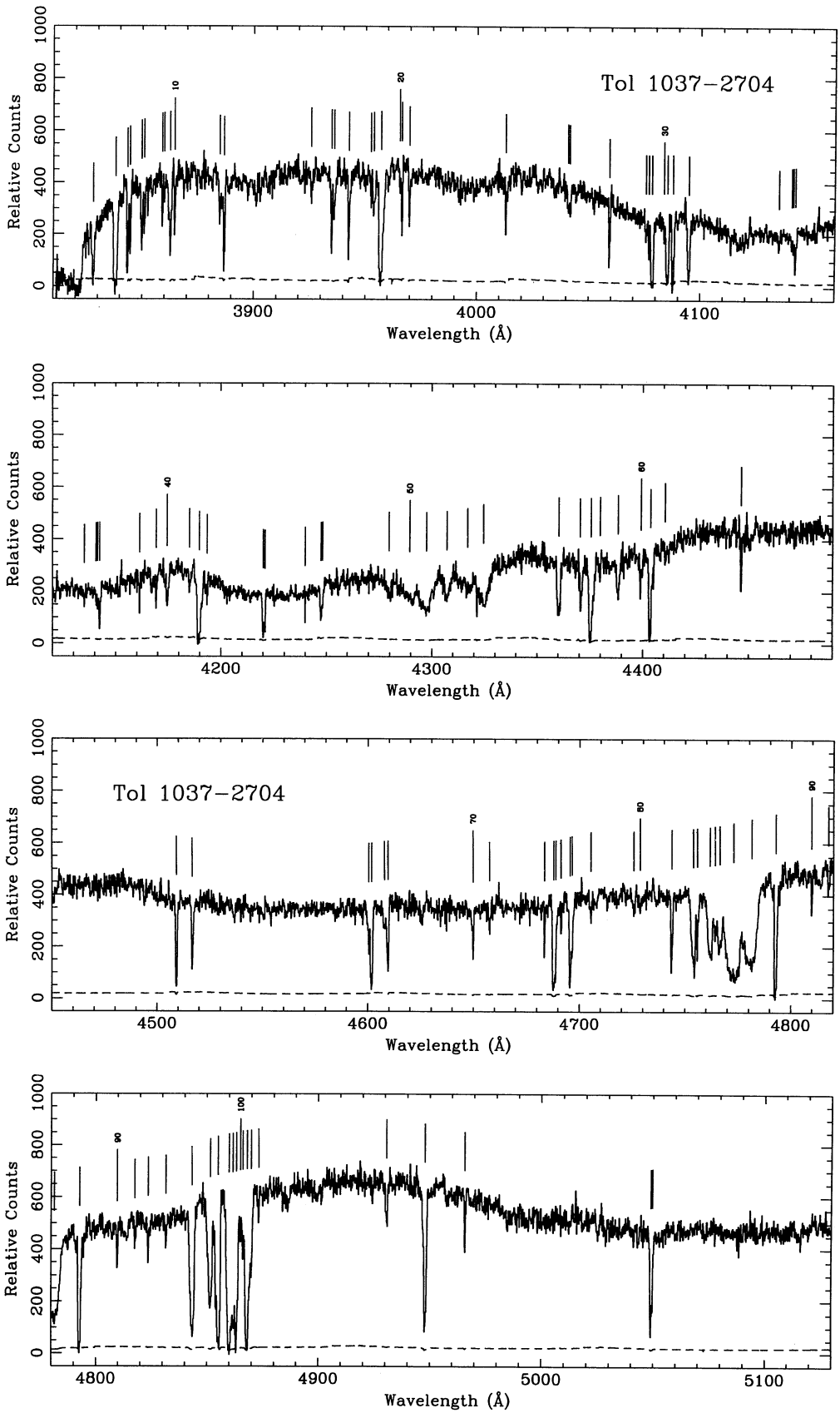

FIG. 2.—CTIO echelle spectra of Tol 1037 − 2704 as a function of vacuum heliocentric wavelength. The dotted line shows the 1 σ errors. The spectral resolution is 30 km s^{-1}. Tick marks indicate all absorption features above the 5 σ equivalent width limit listed in Table 3.

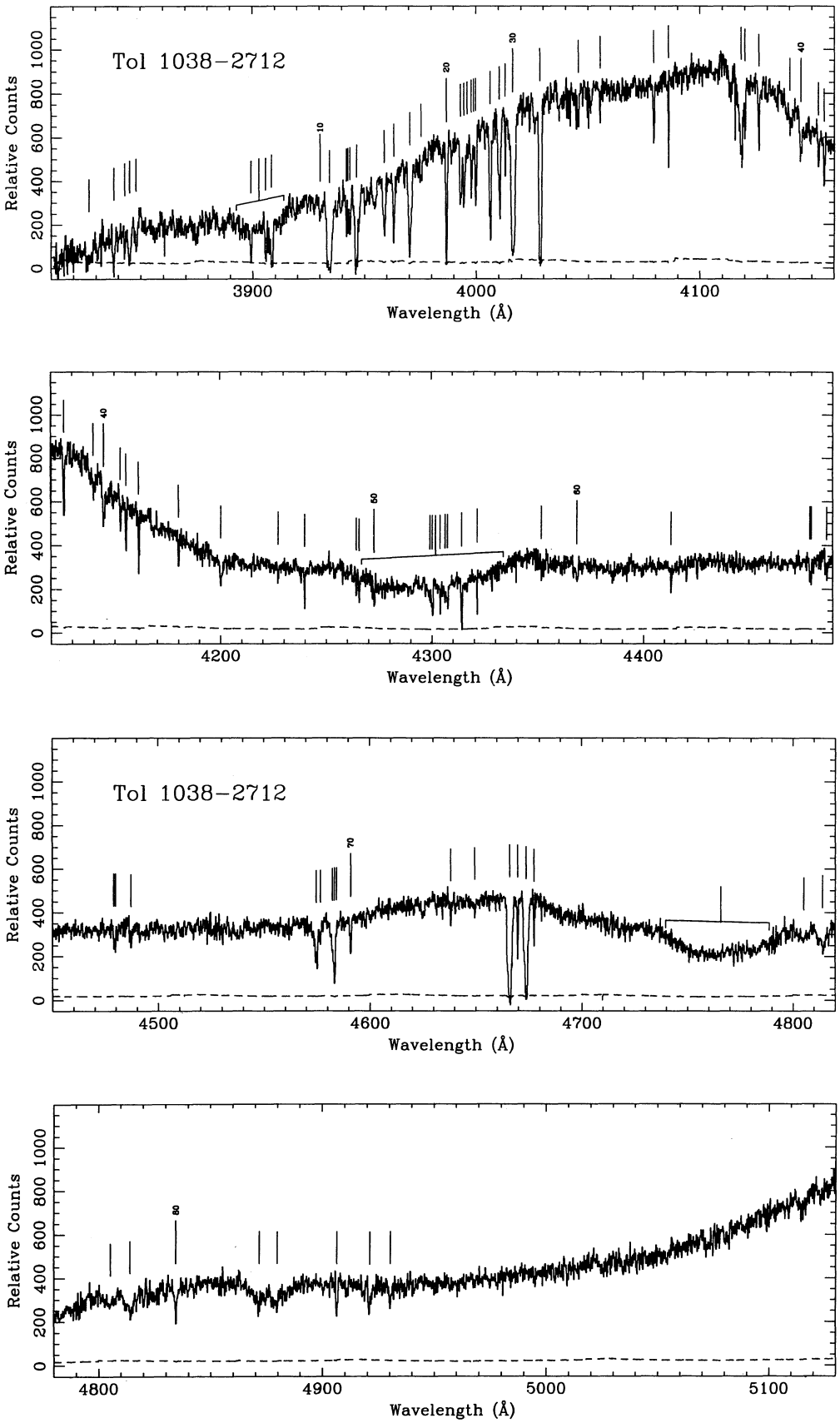

FIG. 3.—Same as Fig. 2 for Tol 1038−2712. Marked features are listed in Table 4.

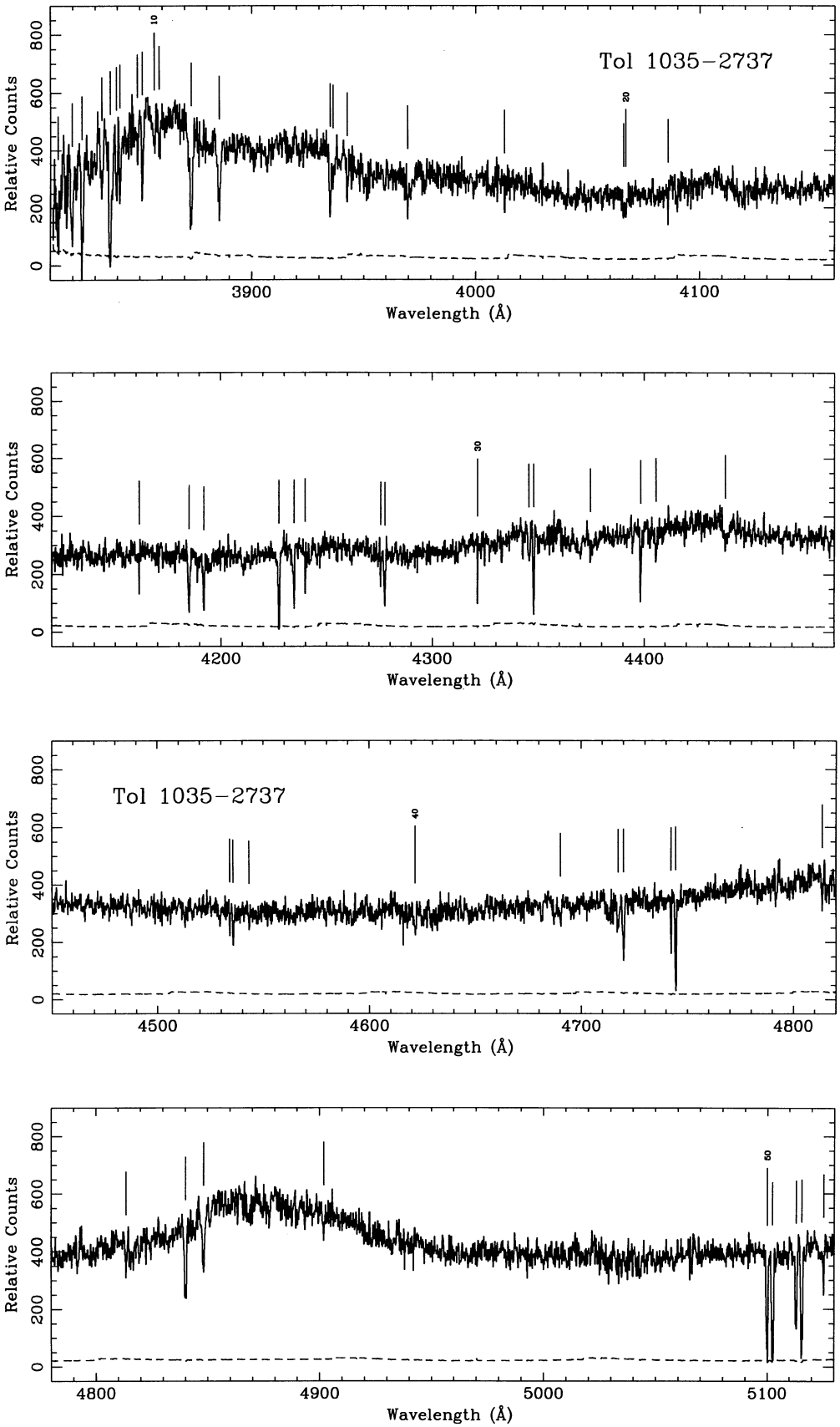

FIG. 4.—Same as Fig. 2 for Tol 1035 − 2737. Marked features are listed in Table 5.

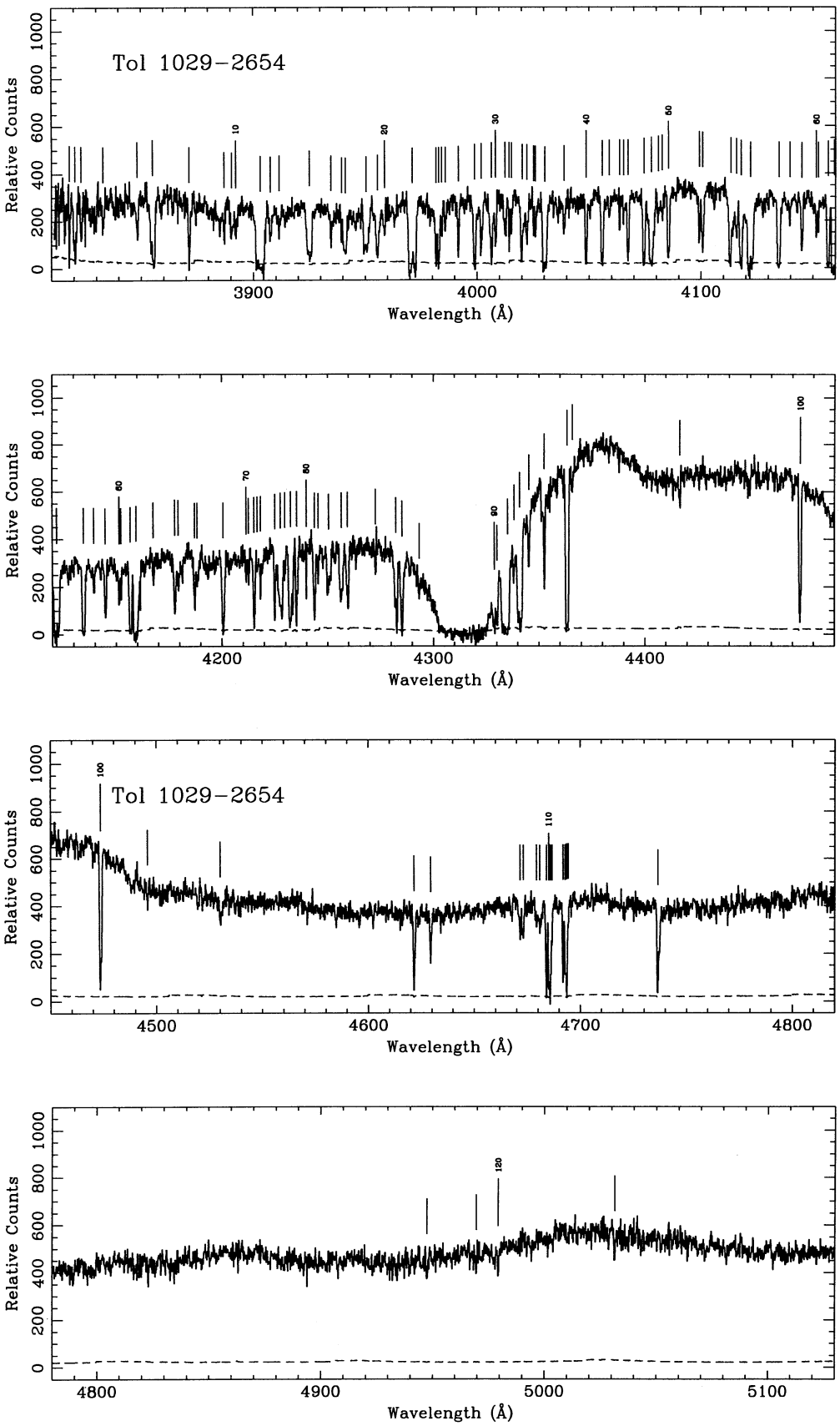

FIG. 5.—Same as Fig. 2 for Tol 1029−2654. Marked features are listed in Table 6.

TABLE 3

ABSORPTION LINES OF TOLOLO 1037−2704

No.	λ_{obs}(Å)	$\sigma(\lambda)$	W_{obs}(Å)	$\sigma(W)$	S/N	ID	z_{abs}	Notes
1	3827.95	0.03	0.91	0.05	17.2	Lyα	2.14884	
2	3837.98	0.06	1.86	0.07	28.3	Lyα	2.15709	
3	3843.38	0.01	0.59	0.03	21.4	C IV 1548	1.48248	
4	3844.53	0.02	0.40	0.03	14.8	C IV 1548	1.48322	
5	3849.74	0.02	0.46	0.03	17.0	C IV 1550	1.48246	
6	3850.92	0.02	0.31	0.03	11.7	C IV 1550	1.48323	
7	3858.95	0.02	0.19	0.02	9.7	Lyα	2.17434	
8	3859.86	0.04	0.12	0.02	5.5	Lyα	2.17509	
9	3862.51	0.02	0.71	0.03	27.5	Lyα	2.17727	
10	3864.56	0.02	0.29	0.02	15.3	Lyα	2.17895	
11	3884.73	0.04	0.24	0.04	6.0	N V 1238	2.13583	a
12	3886.77	0.02	0.59	0.03	17.9	C II 1334	1.91246	
13	3925.76	0.06	0.18	0.03	6.6			
14	3934.82	0.01	0.41	0.02	26.6			
15	3935.97	0.02	0.33	0.02	16.9			
16	3942.58	0.01	0.41	0.02	21.6	Si II 1260	2.12798	
17	3952.56	0.03	0.11	0.02	5.8	Si II 1260	2.13590	
18	3953.84	0.04	0.29	0.03	9.6			
19	3957.12	0.02	1.97	0.04	48.5	Si II 1260	2.13952	b
20	3965.50	0.04	0.09	0.02	5.6	C II 1334	1.97145	
21	3966.35	0.02	0.26	0.02	11.6	C II 1334	1.97209	
22	3969.69	0.02	0.27	0.02	11.5			
23	4012.84	0.01	0.15	0.01	12.5			c
24	4040.77	0.04	0.16	0.02	7.1	C II 1334	2.02785	
25	4041.62	0.03	0.18	0.02	8.2	C II 1334	2.02849	
						Fe II 2382	0.69619	b
26	4059.30	0.01	0.42	0.02	23.1	Si IV 1393	1.91249	
27	4075.72	0.06	0.20	0.03	6.0			
28	4076.98	0.02	0.29	0.02	14.5	C IV 1548	1.63336	
29	4078.48	0.02	1.46	0.03	48.7	C IV 1548	1.63433	
30	4083.83	0.08	0.14	0.02	7.7	C IV 1550	1.63341	
31	4085.28	0.02	1.32	0.03	44.0	C IV 1550	1.63435	b
						Si IV 1402	1.91229	b
32	4087.82	0.02	1.05	0.03	32.1	O I 1302	2.13924	b
33	4094.81	0.03	1.05	0.05	21.1	Si II 1304	2.13930	b
34	4135.09	0.05	0.17	0.03	5.1			
35	4140.82	0.05	0.12	0.02	6.3			
36	4141.47	0.04	0.19	0.04	5.4	Si IV 1393	1.97145	a
37	4142.41	0.02	0.58	0.04	14.3	Si IV 1393	1.97212	
38	4161.39	0.02	0.13	0.02	7.3			c
39	4169.24	0.04	0.28	0.04	7.2	Si IV 1402	1.97215	
40	4174.59	0.05	0.51	0.04	12.0	C II 1334	2.12813	
41	4185.09	0.05	0.18	0.03	5.0	C II 1334	2.13600	
42	4189.77	0.04	2.18	0.06	36.4	C II 1334	2.13950	b
43	4193.54	0.03	0.15	0.03	5.8	C II 1334	2.14233	
44	4220.18	0.03	0.85	0.06	14.7	Si IV 1393	2.02792	
45	4220.96	0.02	0.29	0.05	6.4	Si IV 1393	2.02848	
46	4239.92	0.02	0.16	0.02	8.9			c
47	4247.50	0.04	0.49	0.06	8.5	Si IV 1402	2.02794	
48	4248.24	0.05	0.12	0.02	5.5	Si IV 1402	2.02847	
49	4279.79	0.12	0.90	0.07	13.1	Si IV 1393	2.07069	
50	4289.57	0.32	2.93	0.23	12.8	Si IV 1393	2.07771	b
51	4297.61	0.13	2.67	0.20	13.1	Si IV 1393	2.08348	
52	4307.15	0.08	0.86	0.05	16.1	Si IV 1402	2.07046	
53	4316.95	0.40	1.52	0.22	6.8	Si IV 1402	2.07745	b
54	4324.55	0.16	2.55	0.20	12.9	Si IV 1402	2.08286	
55	4360.24	0.03	1.06	0.03	35.3	Si IV 1393	2.12841	
56	4370.85	0.04	0.68	0.03	20.0	Si IV 1393	2.13601	
57	4375.59	0.02	2.09	0.03	69.6	Si IV 1393	2.13943	b
58	4379.74	0.04	0.11	0.02	5.7	Si IV 1393	2.14240	a
59	4388.36	0.04	0.63	0.03	21.4	Si IV 1402	2.12835	b
						Fe II 2586	0.69654	b

TABLE 3—*Continued*

No.	λ_{obs}(Å)	$\sigma(\lambda)$	W_{obs}(Å)	$\sigma(W)$	S/N	ID	z_{abs}	Notes
60	4399.20	0.06	0.36	0.03	10.6	Si IV 1402	2.13608	
61	4403.76	0.02	1.54	0.03	51.3	Si IV 1402	2.13933	b
62	4410.71	0.04	0.07	0.01	5.4	Fe II 2600	0.69631	
63	4446.57	0.02	0.28	0.02	15.5	Si II 1526	1.91252	
64	4509.18	0.01	0.76	0.03	27.5	C IV 1548	1.91253	
65	4516.67	0.02	0.65	0.03	20.3	C IV 1550	1.91253	
66	4600.45	0.06	0.48	0.06	7.9	C IV 1548	1.97148	
67	4601.75	0.03	1.01	0.06	16.8	C IV 1548	1.97232	
68	4607.83	0.10	0.38	0.06	6.8	C IV 1550	1.97131	
69	4609.45	0.03	0.68	0.05	14.7	C IV 1550	1.97235	
70	4649.79	0.02	0.26	0.03	9.0	C IV 1548	2.00335	
71	4657.56	0.05	0.20	0.02	9.4	C IV 1550	2.00338	
72	4683.44	0.01	0.22	0.02	13.3	C IV 1548	2.02508	
73	4687.72	0.02	0.97	0.06	16.2	C IV 1548	2.02785	
74	4688.67	0.03	0.66	0.06	11.5	C IV 1548	2.02846	
75	4691.26	0.02	0.11	0.02	7.0	C IV 1550	2.02511	
76	4695.50	0.02	0.87	0.05	17.6	C IV 1550	2.02782	
77	4696.46	0.03	0.44	0.05	8.9	C IV 1550	2.02846	
78	4705.23	0.05	0.18	0.02	6.4	C IV 1548	2.03915	a
79	4725.65	0.11	0.18	0.03	6.2			
80	4728.64	0.06	0.11	0.02	5.0			
81	4743.70	0.01	0.59	0.02	33.8	Mg II 2796	0.69639	
82	4753.90	0.05	1.67	0.04	43.5	C IV 1548	2.07059	
83	4755.72	0.02	0.55	0.03	21.9	Mg II 2803	0.69633	
84	4761.81	0.03	1.43	0.04	35.8	C IV 1550	2.07060	b
85	4764.06	0.05	0.69	0.03	23.0	C IV 1548	2.07716	b
86	4766.26	0.04	1.23	0.05	24.9	C IV 1548	2.07858	b
87	4772.74	0.05	7.61	0.13	59.7	C IV 1550	2.07765	b
						C IV 1548	2.08276	b
88	4781.35	0.05	3.75	0.10	39.0	C IV 1550	2.08320	b
89	4792.73	0.01	1.38	0.02	69.0	Si II 1526	2.13926	b
90	4809.69	0.03	0.19	0.02	9.2	C IV 1548	2.10663	
91	4817.69	0.03	0.11	0.02	6.4	C IV 1550	2.10664	
92	4823.60	0.02	0.17	0.02	9.5	C IV 1548	2.11561	
93	4831.61	0.02	0.12	0.02	7.9	C IV 1550	2.11561	
94	4843.36	0.02	1.82	0.03	66.6	C IV 1548	2.12838	
95	4851.47	0.02	1.47	0.03	49.8	C IV 1550	2.12842	
96	4855.04	0.01	2.21	0.03	77.3	C IV 1548	2.13592	
97	4859.99	0.03	2.37	0.05	47.4	C IV 1548	2.13912	
98	4861.69	0.07	0.63	0.03	20.1	C IV 1548	2.14022	
99	4863.20	0.06	1.80	0.06	27.8	C IV 1550	2.13598	
100	4865.05	0.04	0.23	0.03	8.8	C IV 1548	2.14238	
101	4866.11	0.03	0.17	0.02	8.3	Al II 1670	1.91247	
102	4868.03	0.02	2.12	0.05	44.1	C IV 1550	2.13910	
103	4869.92	0.03	0.52	0.04	12.9	C IV 1550	2.14032	
104	4873.25	0.04	0.09	0.01	5.8	C IV 1550	2.14246	
105	4930.69	0.04	0.21	0.02	12.0			
106	4947.84	0.01	1.23	0.02	73.4			
107	4965.74	0.02	0.18	0.01	15.6	Al II 1670	1.97210	
108	5049.05	0.03	0.57	0.06	9.5	Fe II 1608	2.13908	
109	5049.77	0.04	0.42	0.06	7.0			

[a] Doublet component below 5 σ equivalent width threshold.
[b] Probable blend.
[c] Possible spurious line.
[d] Probable chance coincidence.

3. IDENTIFICATION OF ABSORPTION LINES

We wrote a search program adopting elements of the algorithms described in Bahcall (1968), Aaronson, McKee, and Weisheit (1975), and Young et al. (1979) to identify the absorption lines automatically. For all observed lines λ_i, all possible redshifts $z_{ij} = \lambda_i/\Lambda_j - 1$ were calculated using a standard set of laboratory wavelengths Λ_j. The redshift range spanned by the z_{ij}-values was then divided into redshift intervals of varying width $\Delta z = (2\delta/3\lambda_c)(1 + z_n)$, where δ is the search acceptance window (0.15 Å) and λ_c is the central wavelength of the spectra (Young et al. 1982). Finally, the number $N(z_n, \delta z)$ of redshifts z_{ij} lying within each interval $z_n \pm 2\Delta z$ was counted and those intervals where $N(z_n, \delta z)$ exceeded a certain threshold value were flagged as a possible candidate system. The fact that the intervals overlapped ensured that no systems were missed because of an unfortunate choice of bins. In the automated search, we used a "short" list of ultraviolet absorption lines corresponding to the strongest transitions of the most abun-

TABLE 4

ABSORPTION LINES OF TOLOLO 1038−2712

No.	λ_{obs}(Å)	$\sigma(\lambda)$	W_{obs}(Å)	$\sigma(W)$	S/N	ID	z_{abs}	Notes
1	3826.89	0.14	1.67	0.23	7.4	Lyα	2.14797	
2	3837.96	0.04	1.01	0.08	12.5	Lyα	2.15707	
3	3842.85	0.03	0.41	0.05	7.6	Lyα	2.16110	
4	3844.99	0.04	1.07	0.07	15.1	Lyα	2.16286	
5	3847.84	0.07	0.60	0.07	15.8	Lyα	2.16520	
6	3899.24	0.03	0.62	0.06	10.2	Lyα	2.20748	
7	3904.79	0.17	2.80	0.17	16.5	N V 1238 + 1242	2.14902	b
8	3905.77	0.02	0.56	0.04	12.6	Lyα	2.21285	
9	3908.35	0.03	1.27	0.05	25.4	Lyα	2.21498	
10	3930.19	0.09	0.19	0.03	5.8	Lyα	2.23294	
11	3934.28	0.02	2.71	0.05	54.2	Lyα	2.23631	
12	3941.83	0.02	0.22	0.03	8.7	Lyα	2.24252	
13	3942.53	0.03	0.17	0.03	5.7	Lyα	2.24309	
14	3943.37	0.05	0.36	0.06	6.3	C II 1334	1.95487	d
15	3946.40	0.04	1.70	0.06	28.3	Lyα	2.24628	
16	3958.79	0.04	0.61	0.04	16.2	Lyα	2.25646	
17	3963.04	0.02	0.52	0.03	18.4	Lyα	2.25996	
18	3970.31	0.02	1.19	0.03	39.4	Lyα	2.26594	
19	3975.31	0.05	0.16	0.02	8.0	Lyα	2.27006	
20	3986.68	0.01	0.80	0.02	49.6	Lyα	2.27941	
21	3992.97	0.02	0.52	0.02	26.9	Lyα	2.28458	
22	3994.45	0.02	0.54	0.02	28.0	Lyα	2.28580	
23	3995.99	0.10	0.17	0.03	5.1	Lyα	2.28707	
24	3997.79	0.02	0.34	0.02	16.1	Lyα	2.28855	
25	3998.77	0.04	0.08	0.01	8.0	Lyα	2.28935	
26	3999.73	0.01	0.40	0.02	21.1	Lyα	2.29014	
27	4006.23	0.01	0.76	0.02	45.1	Lyα	2.29549	
28	4010.30	0.02	0.68	0.02	34.0	Lyα	2.29884	
29	4012.90	0.01	0.10	0.01	9.9	Lyα	2.30098	
30	4016.33	0.03	1.92	0.04	50.9	Lyα	2.30380	
31	4028.45	0.02	1.39	0.02	56.1	Lyα	2.31377	
32	4045.58	0.04	0.08	0.01	5.1	Lyα	2.32786	
33	4055.31	0.03	0.07	0.01	5.9	Lyα	2.33586	
34	4079.25	0.02	0.19	0.01	16.1			
35	4085.82	0.01	0.14	0.01	17.6			
36	4118.38	0.04	0.88	0.04	24.9	Si IV 1393	1.95488	
37	4120.07	0.02	0.10	0.02	6.0	Si IV 1393	1.95609	a
38	4126.22	0.02	0.18	0.01	15.4	Si IV 1393	1.96051	
39	4140.12	0.03	0.06	0.01	5.9			
40	4145.00	0.04	0.28	0.02	12.9	Si IV 1402	1.95487	
41	4152.90	0.04	0.11	0.01	7.4	Si IV 1402	1.96050	
42	4155.47	0.02	0.21	0.01	15.5			
43	4161.47	0.01	0.17	0.01	15.2			
44	4180.22	0.04	0.13	0.02	6.3			
45	4200.32	0.05	0.36	0.03	11.8	Si IV 1393	2.01367	
46	4227.43	0.04	0.11	0.02	5.7	Si IV 1402	2.01363	
47	4239.90	0.02	0.25	0.02	13.5			
48	4264.40	0.04	0.14	0.02	5.6	C IV 1548	1.75442	a
49	4265.78	0.04	0.25	0.04	6.4	C IV 1548	1.75531	
50	4272.83	0.03	0.25	0.04	6.4	C IV 1550	1.75529	
51	4299.18	0.08	0.26	0.03	9.8	C IV 1548	1.77689	
52	4300.34	0.08	0.51	0.03	19.9	C IV 1548	1.77763	
53	4301.84	0.24	11.39	0.19	59.9	Si IV 1393 + 1402	2.07656	b
54	4304.09	0.05	0.31	0.04	8.0			
55	4306.32	0.05	0.25	0.03	10.1	C IV 1550	1.77688	
56	4307.49	0.05	0.44	0.03	15.2	C IV 1550	1.77764	
57	4314.17	0.01	0.63	0.02	25.6			
58	4321.47	0.01	0.17	0.02	9.4			c
59	4351.88	0.04	0.11	0.02	5.6	Si II 1526	1.85050	d
60	4368.72	0.07	0.23	0.04	6.4			
61	4413.27	0.03	0.21	0.03	8.2	C IV 1548	1.85058	a
62	4479.09	0.04	0.13	0.02	5.4	C IV 1548	1.89309	a

TABLE 4—*Continued*

No.	λ_{obs}(Å)	$\sigma(\lambda)$	W_{obs}(Å)	$\sigma(W)$	S/N	ID	z_{abs}	Notes
63	4479.79	0.03	0.15	0.02	6.8	C IV 1548	1.89354	
64	4487.20	0.04	0.13	0.02	6.2	C IV 1550	1.89352	
65	4574.80	0.03	0.87	0.04	23.9	C IV 1548	1.95491	
66	4576.66	0.04	0.13	0.02	6.3	C IV 1548	1.95611	
67	4582.40	0.03	0.61	0.04	14.4	C IV 1550	1.95491	b
68	4583.37	0.02	0.51	0.03	15.8	C IV 1548	1.96045	b
69	4584.26	0.04	0.07	0.02	5.0	C IV 1550	1.95611	
70	4590.99	0.02	0.35	0.02	15.6	C IV 1550	1.96045	
71	4638.29	0.03	0.10	0.02	6.7			
72	4649.63	0.09	0.10	0.02	5.0			
73	4665.98	0.01	2.39	0.03	95.2	C IV 1548	2.01381	
74	4669.74	0.01	0.27	0.01	21.0	C IV 1548	2.01623	
75	4673.68	0.01	1.89	0.02	81.7	C IV 1550	2.01377	
76	4677.48	0.01	0.17	0.01	13.6	C IV 1550	2.01622	
77	4765.69	0.22	11.51	0.16	71.9	C IV 1548 + 1550	2.07662	b
78	4805.20	0.31	0.65	0.09	7.2	Si II 1526	2.14743	
79	4814.01	0.17	1.34	0.09	14.4			
80	4834.50	0.03	0.34	0.03	13.4	Al II 1670	1.89355	d
81	4871.69	0.13	1.31	0.06	21.8	C IV 1548	2.14668	
82	4879.80	0.11	1.26	0.06	21.3	C IV 1550	2.14669	
83	4906.50	0.04	0.29	0.03	9.2			
84	4921.21	0.07	0.42	0.04	10.5			
85	4930.33	0.07	0.26	0.03	8.7			

[a] Doublet component below 5 σ equivalent width threshold.
[b] Probable blend.
[c] Possible spurious line.
[d] Probable chance coincidence.

dant elements (see Morton, York, & Jenkins 1988, Table 4). This list was expanded to include many more lines once a candidate system was accepted.

Once all the candidate systems were identified, we assessed the validity of each candidate according to the probability that the system could have arisen by chance. The statistical analysis adopted is described in detail by Young et al. (1979). Wavelength discrepancies of less than 3 times the estimated 1 σ uncertainty in the wavelength determination were considered acceptable in the line identifications. In almost all cases, the wavelength calibration was of sufficient quality that there was little ambiguity over whether the line belonged to a given redshift system, and few candidate systems were rejected because of a poor wavelength match. For the broad absorption systems, we relaxed the rule to allow wavelength discrepances of as much as 5–6 σ since the uncertainties of these systems are probably underestimated. We also checked to make sure that the doublet ratios agreed with expectation, and the relative strengths of the lines of a given ion agreed with their known oscillator strengths.

This procedure successfully found all the systems with more than two lines, but was insensitive to systems where only the C IV $\lambda\lambda$1548, 1550 or Mg II $\lambda\lambda$2786, 2803 doublet was present. For this reason, manual searches were made for doublets of C IV, Mg II, N V $\lambda\lambda$1238, 1242, and Si IV $\lambda\lambda$1393, 1402, and as well as the Fe II lines. We also made special searches for pairs of O I λ1302 and Si II λ1304, which have a similar wavelength separation as the C IV doublet. In order to minimize the number of misidentifications, we required that for a O I λ1302/Si II λ1304 identification to be accepted, C II λ1334 or Si II λ1260 must be present at the redshifts of the O I and Si II lines. Otherwise, the C IV identification was accepted. Tables 3–6 list the suggested identifications for Tol 1037−2704, Tol 1038−2712, Tol 1035−2737, and Tol 1029−2654, respectively.

4. THE INDIVIDUAL QUASARS AND THEIR ABSORPTION LINE SYSTEMS

The increased resolution of our new observations allows us to confirm many of the identifications made by J86 and S87 and to identify a number of new absorption systems. At the resolution of our data, many of the C IV systems are split into narrower components with velocity separations ranging from about 50–1000 km s^{-1}. In total, we found or confirmed 23 C IV systems in Tol 1037−2704 and 13 systems in Tol 1038−2712 in the redshift range $1.41 \lesssim z \lesssim 2.15$, and discovered two Mg II systems in Tol 1037−2704. In addition, we identified five C IV systems and two Mg II systems in Tol 1035−2737 and six C IV systems in Tol 1029−2654. Of the 47 C IV systems found along the four lines of sight, we think that a maximum of only three could be spurious.

4.1. *Tololo 1037−2704*

The spectrum of Tol 1037−2704 (z_{em} = 2.193) is shown in Figure 2. We call particular attention to the two strong absorption complexes near 4750 and 4900 Å, which appear broad and troughlike in low-resolution data. At 2 Å resolution, S87 were able to decompose the 4750 Å complex into three components and the 4900 Å complex into two components. In our data, we identified four components near 4750 Å and five components near 4900 Å. S87 have used the fact that the broad lines resolve into finer structure at high resolution to argue that Tol 1037−2704 is not a broad absorption line (BAL) QSO. Although the features in the spectrum of Tol 1037−2704 do not remain broad and troughlike at high resolution, BAL QSOs with complex absorption structure are not unknown. Weymann et al. (1981) have defined a subclass of QSOs showing complex structure in their BAL troughs. The BAL QSO 1303+308 is an extreme example of this class of QSO (Foltz et al. 1987), although Romani, Filippenko, & Steidel

TABLE 5

ABSORPTION LINES OF TOLOLO 1035−2737

No.	λ_{obs}(Å)	$\sigma(\lambda)$	W_{obs}(Å)	$\sigma(W)$	S/N	ID	z_{abs}	Notes
1	3813.35	0.08	0.79	0.13	6.2	Lyα	2.13683	
2	3819.61	0.05	0.76	0.09	8.8	Lyα	2.14198	
3	3824.10	0.02	1.09	0.06	17.1	Lyα	2.14567	
4	3832.86	0.07	0.38	0.06	6.3	Lyα	2.15288	
5	3836.64	0.02	1.41	0.07	20.2	Lyα	2.15599	
6	3839.46	0.04	0.36	0.04	10.1	Lyα	2.15831	
7	3840.98	0.03	0.38	0.03	11.4	Lyα	2.15956	
8	3848.86	0.04	0.13	0.02	5.5	Lyα	2.16604	
9	3850.97	0.02	0.38	0.03	13.9	Lyα	2.16778	
10	3856.34	0.07	0.18	0.03	5.6	Lyα	2.17219	
11	3858.63	0.05	0.24	0.03	8.1	Lyα	2.17408	
12	3872.86	0.02	0.89	0.05	17.1	N v 1238	2.12625	
13	3885.44	0.05	0.65	0.07	9.5	N v 1242	2.12635	
14	3934.90	0.02	0.49	0.03	14.3			
15	3936.21	0.06	0.22	0.04	5.9			
16	3942.51	0.02	0.14	0.02	8.3			
17	3969.66	0.04	0.30	0.04	7.0			
18	4012.82	0.03	0.13	0.02	5.3			
19	4065.87	0.04	0.20	0.04	5.6			
20	4066.90	0.06	0.22	0.04	5.5			
21	4085.77	0.02	0.12	0.02	5.2			c
22	4161.39	0.02	0.13	0.02	6.8			c
23	4184.98	0.03	0.63	0.05	11.7	C IV 1548	1.70312	
24	4191.96	0.03	0.42	0.04	10.4	C IV 1550	1.70314	
25	4227.48	0.01	0.70	0.03	24.4	C IV 1548	1.73057	
26	4234.54	0.02	0.43	0.03	14.9	C IV 1550	1.73060	
27	4239.89	0.02	0.18	0.02	11.2			c
28	4275.59	0.03	0.16	0.03	6.2	Fe II 2344	0.82389	
29	4277.55	0.02	0.50	0.04	13.9	Fe II 2344	0.82473	
30	4321.40	0.01	0.18	0.02	10.4			c
31	4345.69	0.07	0.27	0.05	5.7	Fe II 2382	0.82380	
32	4347.86	0.02	0.57	0.04	14.1	Fe II 2382	0.82471	b
33	4374.51	0.03	0.09	0.02	5.4			c
34	4398.22	0.02	0.43	0.02	19.0	C IV 1548	1.84086	
35	4405.59	0.04	0.22	0.03	8.7	C IV 1550	1.84090	
36	4438.30	0.10	0.25	0.05	5.0			
37	4534.11	0.04	0.10	0.02	5.2			
38	4535.71	0.03	0.26	0.03	8.6	C IV 1548	1.92966	
39	4543.19	0.05	0.12	0.03	5.0	C IV 1550	1.92963	
40	4621.73	0.07	0.21	0.04	5.3			
41	4690.30	0.07	0.16	0.03	5.2			
42	4717.46	0.07	0.36	0.04	8.1	Fe II 2586	0.82377	
43	4720.00	0.03	0.52	0.04	12.7	Fe II 2586	0.82475	
44	4742.35	0.02	0.22	0.02	11.7	Fe II 2600	0.82386	
45	4744.57	0.01	0.73	0.02	30.3	Fe II 2600	0.82471	
46	4813.59	0.06	0.16	0.03	5.4			
47	4840.20	0.02	0.58	0.03	21.5	C IV 1548	2.12634	
48	4848.22	0.03	0.40	0.03	13.5	C IV 1550	2.12632	
49	4901.98	0.07	0.12	0.02	6.0			
50	5100.02	0.01	0.86	0.03	31.0	Mg II 2796	0.82381	
51	5102.44	0.01	1.11	0.03	33.6	Mg II 2796	0.82468	
52	5113.07	0.02	0.61	0.03	21.5	Mg II 2803	0.82380	
53	5115.52	0.01	0.97	0.02	29.5	Mg II 2803	0.82467	
54	5125.37	0.03	0.20	0.02	8.3			

[a] Doublet component below 5 σ equivalent width threshold.
[b] Probable blend.
[c] Possible spurious line.
[d] Probable chance coincidence.

(1991) suggest that it might be another example of superclustered absorption. On this basis, the classification of this QSO as BAL is still unclear.

z_{abs} = 0.69636.—This strong, certain Mg II system was previously unidentified, perhaps because the Mg II λ2803 line is blended with the C IV λ1548 line of the z_{abs} = 2.07059 system. The Fe II λλ2586, 2600 lines appear to be present with the former blended with Si IV λ1402 of the z_{abs} = 2.12815 system. The line identified as Fe II λ2382 has also been identified as C II λ1334 of system z_{abs} = 2.02847.

The following two systems are members of a newly identified C IV complex in the Lyα forest. The probability of getting C IV doublet-like matches in the Lyα forest by chance is $\lesssim$0.008.

z_{abs} = 1.48248.—The identification of this system is based

TABLE 6

ABSORPTION LINES OF TOLOLO 1029−2654

No.	λ_{obs}(Å)	$\sigma(\lambda)$	W_{obs}(Å)	$\sigma(W)$	S/N	ID	z_{abs}	Notes
1	3817.90	0.02	0.39	0.04	8.7	Lyα	2.14057	
2	3820.44	0.05	1.07	0.08	13.4	Lyα	2.14266	
3	3823.16	0.05	0.39	0.06	6.7	Lyα	2.14490	
4	3832.87	0.08	0.31	0.05	5.8	Lyα	2.15289	
5	3848.18	0.04	0.43	0.04	11.5	Lyα	2.16548	
6	3855.10	0.03	1.96	0.05	39.2	Lyα	2.17117	
7	3871.39	0.02	0.82	0.04	20.4	Lyα	2.18457	
8	3887.01	0.04	0.26	0.04	5.9	Lyα	2.19742	
9	3890.31	0.06	0.50	0.06	8.2	Lyα	2.20014	
10	3892.18	0.05	0.32	0.05	6.7	Lyα	2.20167	
11	3903.09	0.04	4.26	0.09	47.3	Lyα	2.21065	
12	3907.56	0.05	0.38	0.05	8.3	Lyα	2.21432	
13	3911.47	0.06	0.23	0.05	5.1	Lyα	2.21754	
14	3925.07	0.06	2.10	0.07	28.7	Lyα	2.22873	
15	3934.74	0.03	0.34	0.04	9.8	Lyα	2.23668	
16	3939.49	0.03	0.23	0.03	7.7	Lyα	2.24059	
17	3941.18	0.04	1.05	0.05	19.8	Lyα	2.24198	
18	3950.48	0.06	1.58	0.09	17.6	Lyα	2.24963	
19	3955.50	0.04	1.07	0.06	17.5	Lyα	2.25376	
20	3958.61	0.07	0.35	0.06	5.7	Lyα	2.25632	
21	3971.08	0.03	3.69	0.07	95.6	Lyα	2.26658	
22	3981.61	0.02	0.76	0.05	13.9	Lyα	2.27524	
23	3982.78	0.02	1.02	0.06	16.6	Lyα	2.27620	
24	3984.07	0.05	0.34	0.04	9.5	Lyα	2.27726	
25	3985.73	0.03	0.28	0.03	9.1	Lyα	2.27863	
26	3991.62	0.02	0.60	0.03	18.3	Lyα	2.28347	
27	3998.84	0.01	1.17	0.03	40.3	Lyα	2.28941	
28	4001.84	0.02	0.76	0.03	23.5	Lyα	2.29188	
29	4006.39	0.02	1.14	0.03	33.8	Lyα	2.29562	
30	4008.22	0.03	0.56	0.03	17.4	Lyα	2.29713	
31	4012.52	0.04	0.52	0.04	13.2	Lyα	2.30067	
32	4014.38	0.02	0.37	0.04	10.0	Lyα	2.30220	
33	4015.34	0.05	0.28	0.05	5.7	Lyα	2.30298	
34	4020.16	0.05	1.10	0.06	18.3	Lyα	2.30695	
35	4022.25	0.04	0.54	0.05	11.0	Lyα	2.30867	
36	4025.23	0.03	0.23	0.04	6.2	Lyα	2.31112	
37	4026.07	0.04	0.31	0.04	7.0	Lyα	2.31181	
38	4030.17	0.03	2.09	0.06	34.8	Lyα	2.31518	
39	4038.84	0.05	0.38	0.05	7.3	C II 1334	2.02641	d
40	4048.61	0.02	0.82	0.03	26.8	Lyα	2.33035	
41	4055.76	0.02	1.13	0.03	33.1	Lyα	2.33623	
42	4058.90	0.05	0.20	0.03	7.1	Lyα	2.33882	
43	4063.51	0.02	0.18	0.02	8.4	Lyα	2.34261	
44	4065.21	0.03	0.19	0.03	7.5	Lyα	2.34401	
45	4067.24	0.02	0.83	0.03	29.4	Lyα	2.34568	
46	4074.39	0.02	1.19	0.03	36.7	Lyα	2.35156	
47	4077.68	0.02	2.22	0.04	58.0	Lyα	2.35427	
48	4080.75	0.06	0.30	0.04	7.6	Lyα	2.35679	
49	4082.52	0.06	0.33	0.04	7.5	Lyα	2.35825	
50	4085.36	0.02	1.00	0.03	29.4	Lyα	2.36058	
51	4099.10	0.03	0.51	0.04	11.7	Lyα	2.37189	
52	4100.63	0.03	0.89	0.07	12.9	Lyα	2.37314	
53	4113.23	0.03	1.68	0.05	33.6	Lyα	2.38351	
54	4115.70	0.05	0.69	0.07	9.3	Lyα	2.38554	
55	4117.79	0.02	1.47	0.04	39.1	Lyα	2.38726	
56	4121.98	0.02	2.86	0.05	57.2	Lyα	2.39071	
57	4134.68	0.04	1.54	0.05	33.1	Lyα	2.40115	
58	4139.53	0.03	0.23	0.03	8.1	Lyα	2.40514	
59	4144.95	0.02	0.61	0.03	23.3	Lyα	2.40960	
60	4151.48	0.03	0.41	0.03	12.5	Lyα	2.41497	
61	4152.37	0.02	0.20	0.03	8.0	Lyα	2.41570	
62	4156.77	0.02	1.41	0.03	42.2	Lyα	2.41932	

TABLE 6—*Continued*

No.	λ_{obs}(Å)	$\sigma(\lambda)$	W_{obs}(Å)	$\sigma(W)$	S/N	ID	z_{abs}	Notes
63	4159.52	0.02	2.86	0.04	48.5	Lyα	2.42159	
64	4167.67	0.05	0.19	0.03	5.6	Lyα	2.42829	
65	4177.79	0.04	0.79	0.06	12.8	Lyα	2.43661	
66	4179.49	0.08	0.54	0.07	7.4	Lyα	2.43801	
67	4187.14	0.03	0.48	0.04	10.9	Lyα	2.44431	
68	4188.50	0.08	0.31	0.06	5.5	Lyα	2.44542	
69	4200.66	0.02	1.21	0.03	38.3	Lyα	2.45543	
70	4211.65	0.04	0.19	0.03	7.5	Lyα	2.46447	
71	4212.74	0.03	0.18	0.02	7.4	Lyα	2.46536	
72	4215.34	0.01	0.80	0.03	29.8	Lyα	2.46750	
73	4216.84	0.06	0.15	0.03	5.4	Si IV 1393	2.02552	
74	4218.34	0.02	0.25	0.03	8.5	Si IV 1393	2.02660	
75	4225.13	0.02	0.64	0.02	32.0	Si II 1190	2.54929	
76	4227.72	0.02	1.65	0.03	55.1	Lyα	2.47769	
77	4229.77	0.04	0.26	0.02	13.2	Lyα	2.47937	
78	4232.58	0.02	1.77	0.03	59.5	Lyα	2.48168	
79	4235.36	0.02	0.78	0.02	39.4	Si II 1193	2.54931	
80	4239.92	0.01	0.15	0.01	12.2	Lyα	2.48772	
81	4243.82	0.01	0.77	0.02	33.0	Si IV 1402	2.02531	
82	4245.61	0.02	0.15	0.02	7.6	Si IV 1402	2.02659	b
83	4250.57	0.04	0.82	0.05	16.4	Lyα	2.49648	
84	4256.61	0.03	0.92	0.04	23.6	Lyα	2.50145	
85	4259.55	0.04	0.76	0.04	19.9	Lyα	2.50387	
86	4272.75	0.03	0.14	0.02	6.1	Lyα	2.51473	
87	4282.40	0.03	1.28	0.04	32.0	Lyα	2.52267	
88	4285.28	0.03	1.40	0.04	35.5	Lyα	2.52504	
89	4293.36	0.04	0.19	0.03	6.5	Lyα	2.53168	
90	4328.91	0.05	1.07	0.11	9.8	Lyα	2.56092	
91	4330.27	0.04	0.60	0.08	7.3	Lyα	2.56204	
92	4335.26	0.03	3.77	0.07	53.8	Lyα	2.56615	
93	4338.28	0.05	0.32	0.04	7.7	Lyα	2.56863	
94	4340.92	0.03	2.36	0.05	47.2	Lyα	2.57080	
95	4345.32	0.03	0.29	0.03	10.6	Lyα	2.57442	
96	4352.59	0.01	0.50	0.02	23.2	Lyα	2.58040	
97	4363.29	0.01	1.65	0.02	81.6	Lyα	2.58921	
98	4365.74	0.05	0.13	0.02	7.3	Lyα	2.59122	
99	4416.54	0.05	0.11	0.02	5.8			
100	4473.71	0.01	1.01	0.02	61.5	Si II 1260	2.54937	
101	4495.85	0.05	0.09	0.02	5.0			
102	4530.17	0.08	0.26	0.04	5.9			
103	4621.69	0.01	0.75	0.03	25.2	O I 1302	2.54923	
104	4629.42	0.03	0.47	0.03	14.0	Si II 1304	2.54916	
105	4671.60	0.04	0.32	0.03	10.2	C IV 1548	2.01744	
106	4673.09	0.04	0.39	0.04	11.9	C IV 1548	2.01840	
107	4679.36	0.04	0.21	0.03	7.6	C IV 1550	2.01744	
108	4680.86	0.04	0.31	0.03	10.6	C IV 1550	2.01840	
109	4684.07	0.01	0.71	0.02	37.4	C IV 1548	2.02549	
110	4685.11	0.02	0.43	0.05	8.9	C IV 1548	2.02616	
111	4685.81	0.02	0.87	0.06	14.9	C IV 1548	2.02661	
112	4686.65	0.02	0.17	0.02	6.9	C IV 1548	2.02716	
113	4691.85	0.01	0.58	0.02	31.1	C IV 1550	2.02549	
114	4692.90	0.02	0.30	0.04	7.3	C IV 1550	2.02617	
115	4693.60	0.02	0.81	0.05	15.9	C IV 1550	2.02662	
116	4694.43	0.02	0.07	0.01	6.8	C IV 1550	2.02715	
117	4736.54	0.01	0.82	0.02	39.9	C II 1334	2.54921	
118	4947.57	0.07	0.13	0.02	5.4	Si IV 1393	2.54981	
119	4969.70	0.04	0.09	0.02	5.0			
120	4979.53	0.03	0.13	0.02	7.4	Si IV 1402	2.54978	
121	5031.45	0.05	0.10	0.02	5.1			

[a] Doublet component below 5 σ equivalent width threshold.
[b] Probable blend.
[c] Possible spurious line.
[d] Probable chance coincidence.

solely on the presence of the C IV doublet. The components agree within a redshift difference of 0.00002 and have a doublet ratio [DR = $W_0(1548)/W_0(1550)$] of 1.28 ± 0.06.

z_{abs} = 1.48323.—As above, this system is identified by it's C IV doublet, with excellent redshift agreement ($\Delta z \lesssim 0.00001$) and a doublet ratio of DR = 1.29 ± 0.06.

The following two systems are members of a another new C IV complex, identified purely on the basis of the C IV doublet. The probability of getting such matches by chance outside the Lyα forest is small, $\lesssim$0.002.

z_{abs} = 1.63336.—This is the weaker of the two systems. The redshift agreement between the components of the C IV doublet is better than 0.00005.

z_{abs} = 1.63434.—This system is identified solely by its saturated C IV doublet. The C IV λ1550 line was identified as O I λ1302 and Si IV λ1402 of other systems by S87 probably because of inadequate resolution. However, it is clear from our data that the C IV λ1550 of this system and O I λ1302 of the z_{abs} = 2.13928 system are different lines. The Si IV λ1402 line of z_{abs} = 1.91249 is clearly blended and its equivalent width contributes $\lesssim$0.42 Å to the C IV λ1550 line. The redshifts of the doublet components are in excellent agreement ($\Delta z \lesssim 0.00002$).

z_{abs} = 1.91249.—This strong, certain system was identified as z_{abs} = 1.9122 by S87. It consists of the C IV doublet, C II λ1334, Si IV $\lambda\lambda$1393, 1402, Si II λ1526, and Al II λ1670. Fe II λ1608, which was tentatively identified by S87 is not present in our spectrum. The strengths of Si IV $\lambda\lambda$1393 and 1402 are not in their correct ratios; however, Si IV λ1402 appears to be blended with C IV λ1550 of system z_{abs} = 1.63434. Al II λ1670 is clearly present, but blended with the absorption complex at $z_{abs} \sim$ 2.14. Therefore, although its line center is well determined, its equivalent width must be considered approximate.

The following two systems appear as a single system in lower resolution data. They were identified as z_{abs} = 1.9722 by S87. There is some evidence for an even weaker system shortward of the two at $z_{abs} \simeq$ 1.9710 from structure in the C IV doublet and Si IV $\lambda\lambda$1393, 1402 lines.

z_{abs} = 1.97145.—This is a certain system based on the C IV doublet, C II λ1334, and Si IV λ1393. Si IV λ1402 is present at only the 2.8 σ significance level. It is not clear whether Fe II λ1608 is present because it would be blended with the C IV λ1550 line of the z_{abs} = 2.08301 system. This system would have been blended with the stronger absorption system at z_{abs} = 1.97216 in lower resolution data.

z_{abs} = 1.97216.—This is a strong system, identified by S87 as z_{abs} = 1.9722. We can identify the lines of C IV $\lambda\lambda$1548, 1550, Si IV $\lambda\lambda$1393, 1402, C II λ1334, and Al II λ1670. As above, Fe II λ1608 may be present but would be blended with the C IV λ1550 line of the z_{abs} = 2.08301 system.

z_{abs} = 2.00335.—This new C IV system was probably too weak to have been identified by S87. Both components of the doublet are at z_{abs} = 2.00335 ± 0.00003 and the doublet ratio is 1.30 ± 0.04.

The following three systems were identified as one system at z_{abs} = 2.0289 by S87 in their 2 Å resolution spectra. The two strongest systems are severely blended, but all their lines show similar structure.

z_{abs} = 2.02509.—This system is identified by only a weak C IV doublet. The components of the doublet agree within $\Delta z \lesssim 0.00003$ and the doublet ratio is $\sim$2.

z_{abs} = 2.02786.—This system is certain. In addition to the saturated C IV doublet, the lines of C II λ1334 and Si IV $\lambda\lambda$1393, 1402 are identified.

z_{abs} = 2.02847.—This system is also certain and shows the same lines as the z_{abs} = 2.02786 system.

z_{abs} = 2.03915.—This is another weak system identified solely on the presence of the C IV $\lambda\lambda$1548, 1550 lines, with redshift agreement better than 0.00003. C IV λ1550 is present at the 3.3 σ confidence level.

The following complex was identified by S87 as a triple system at z_{abs} = 2.0708, 2.0755, and 2.0825. There is evidence for at least three systems in our spectrum, and probably a fourth from structure in the C IV $\lambda\lambda$1548, 1550, and Si IV $\lambda\lambda$1393, 1402 lines. Many of the lines in these systems are broad and asymmetric, making the line positions and equivalent widths listed in Table 3 uncertain.

z_{abs} = 2.07059.—The strong C IV $\lambda\lambda$1548, 1550 lines are broad and asymmetric, as are the lines of Si IV $\lambda\lambda$1393, 1402. Despite the difficulty in measuring line positions of such broad lines, the redshifts of all the lines associated with this system agree within 0.0002.

z_{abs} = 2.07716.—This probable system is identified from the structure in the C IV doublet lines and is the least certain of this complex. The C IV λ1550 line of the system is severely blended with C IV λ1548 of the z_{abs} = 2.08321 system. The Si IV lines are also blended with those of the z_{abs} = 2.07820 system. The redshift of this system, z_{abs} = 2.07716 ± 0.00003, is based only on the C IV λ1548 line.

z_{abs} = 2.07858.—This certain system is most readily identifiable from the Si IV $\lambda\lambda$1393, 1402 lines, the C IV λ1550 line of the C IV doublet being severely blended with the C IV λ1548 line of the z_{abs} = 2.08321 system. We adopt the redshift of the C IV λ1548 line, z_{abs} = 2.07858 ± 0.00003, for the system.

z_{abs} = 2.08321.—This system is the strongest and broadest of the four systems in this complex. The average FWHM of the C IV doublet lines is $\sim$440 km s^{-1}. The C IV λ1548 line is blended with C IV λ1550 of the above system. Identifications of the C IV and Si IV are certain and their redshifts are in good agreement ($\Delta z \lesssim 0.0006$). The unblended lines give a weighted average redshift of z_{abs} = 2.08321 ± 0.00003 for the system.

z_{abs} = 2.10663.—This probable system was probably not identified in prior studies because of its weakness. It is identified solely on the presence of the C IV doublet. The doublet components match in redshift to within 0.00001.

z_{abs} = 2.11561.—This is another new, weak system identified by C IV $\lambda\lambda$1548, 1550, which match in redshift within $\Delta z \lesssim$ 0.00001.

The following complex was listed as at least two systems (z_{abs} = 2.1283 and 2.1378) by S87. There was also evidence in their data that the second system was further separable into two subsystems at z_{abs} = 2.135 and 2.139. In our spectrum, the complex is clearly separable into four systems with a probable fifth system present.

z_{abs} = 2.12818.—In addition to the strong and broad C IV doublet, we also observe Si II λ1260, C II λ1334, and Si IV $\lambda\lambda$1393, 1402. Si IV λ1402 is blended with Fe II λ2586 of the Mg II system at z_{abs} = 0.69636. All except Si II λ1260 and C II λ1334 agree within 0.00008. The weighted average redshift of the unblended lines is z_{abs} = 2.12818 ± 0.00001.

z_{abs} = 2.13593.—This system is certain. Besides a strong C IV doublet, we see N V λ1238, Si II λ1260, C II λ1334 and Si IV $\lambda\lambda$1393, 1402. N V λ1242 and Si II λ1526 appear to be present below the 5 σ detection level. From the Si IV doublet lines, this system appears to be made up of two subsystems at z_{abs} = 2.13589 and 2.13645.

z_{abs} = 2.13910.—This is another strong, certain system. We

identified Si II λ1260, O I λ1302, Si II λ1304, C II λ1334, Si IV $\lambda\lambda$1393, 1402, Si II λ1526, C IV $\lambda\lambda$1548, 1550, and Fe II λ1608. Many of the lines appear saturated and severely blended with lines associated with the $z_{abs} = 2.14030$ system. The redshift of the system was determined from only the unblended C IV and Fe II lines.

$z_{abs} = 2.14030$.—This system is severely blended with the previous system at $z_{abs} = 2.13928$ but is definitely real. All the lines observed in the above system are present in this system (except Fe II λ1608). No attempt was made to deblend any of the lines, other than C IV $\lambda\lambda$1548, 1550, of the two systems. Therefore, the redshift of this system was determined from the C IV doublet lines alone.

$z_{abs} = 2.14243$.—This system is weak, but certain. It consists of C II λ1334, the C IV doublet, and Si IV λ1393. Si IV λ1402 is present below the 5 σ detection threshold.

4.2. *Tololo 1038−2712*

The spectrum of Tol 1038−2712 ($z_{em} = 2.331$) is shown in Figure 3. It contains broad, troughlike C IV absorption complexes near 4750 and 4900 Å similar to Tol 1037−2704. On this basis, Tol 1038−2712 was classified as a marginal BAL QSO by S87. Even in our high-resolution data, we were not able to resolve the C IV doublet structure in the complex near 4750 Å; nor were we able to resolve the Si IV doublet structure. The classification of this QSO as a BAL QSO remains uncertain.

The lines associated with the following three systems were identified by S87 as Si IV doublets belonging to three C IV systems at $z_{abs} \simeq 2.0652$, 2.0768, and 2.0851. The C IV in their data, as in ours, appeared smooth, and the basis of these identifications was the apparent structure in what they interpreted as Si IV lines. We believe the Si IV doublet associated with C IV at $z_{abs} \simeq 2.07620$ is similarly smooth, and remains unresolved in our data. Furthermore, we believe that the sharp features superposed on the unresolved Si IV are more accurately identified as C IV doublets.

$z_{abs} = 1.75530$.—This is a new system consisting of an isolated C IV doublet with excellent redshift agreement ($\Delta z \lesssim 0.00002$). There is evidence for a weaker system at $z_{abs} = 1.75442$. The C IV λ1550 line was identified as Si IV λ1393 from a system identified by S87 as $z_{abs} = 2.0652$.

$z_{abs} = 1.77688$.—This is a new weak system consisting of the C IV doublet. C IV λ1550 is blended or affected by a noise spike, but the doublet lines nevertheless show good redshift agreement ($\Delta z \lesssim 0.00001$).

$z_{abs} = 1.77764$.—This new system is relatively strong. The C IV $\lambda\lambda$1548, 1550 lines show evidence of structure. The redshift agreement between the doublet lines is $\Delta z \lesssim 0.00001$. The C IV λ1548 line was identified as Si IV λ1402 of the system $z_{abs} = 2.0646$ and Si IV λ1393 of $z_{abs} = 2.0845$.

$z_{abs} = 1.85055$.—This system was classified as marginal by S87. The C IV doublet is extremely weak, with the C IV λ1550 line present at only the 4.5 σ confidence level. Nevertheless, given that the redshift difference between the doublet components is so small, less than 0.00001, this system is likely real. Si II λ1526 appears to be present at the 5.6 σ level. If the Si IV doublet is present, the lines are obscured by blending in the Lyα forest.

The following complex was identified as a single system ($z_{abs} = 1.8936$) and classified as marginal by S87. In our spectrum, the complex is clearly split into two systems.

$z_{abs} = 1.89309$.—This system is identified solely by the presence of a very weak C IV λ1548. The C IV λ1550 line falls below the 5 σ equivalent width threshold.

$z_{abs} = 1.89353$.—This is the stronger member of the pair. Both C IV doublet lines are present above the 6 σ confidence level. The line identified as Al II λ1670 is considerably stronger than the C IV doublet and its identification remains uncertain.

The following complex has been divided into three subsystems based on the structure in the C IV and Si IV doublet lines.

$z_{abs} = 1.95489$.—This strong system was identified by S87 as $z_{abs} = 1.955$. The C IV and Si IV doublets show evidence for structure with possible subsystems at $z_{abs} = 1.9543$, 1.9547, and 1.9551. The C IV λ1550 line is severely blended with the C IV λ1548 line of the $z_{abs} = 1.96047$ system. The line we identify as C II λ1334 lies in the Lyα forest and is almost certainly a chance coincidence.

$z_{abs} = 1.95610$.—This system is certain, although the C IV doublet is weak and the C IV λ1550 line severely blended with the C IV λ1548 line of the $z_{abs} = 1.96047$ system. The Si IV λ1393 line is present at the 6 σ confidence level, but Si IV λ1402 falls below the 5 σ threshold.

$z_{abs} = 1.96047$.—This is a certain system. Besides the C IV doublet, the Si IV $\lambda\lambda$1393, 1402 lines are clearly present. The C IV λ1548 line is blended with the C IV λ1550 lines of the $z_{abs} = 1.95489$ and $z_{abs} = 1.95610$ systems.

The following strong and certain complex consists of two subsystems at $z_{abs} = 2.01378$ and $z_{abs} = 2.01623$. S87 identified this complex as one system at $z_{abs} = 2.0144$.

$z_{abs} = 2.01378$.—This strong system consists of the C IV $\lambda\lambda$1548, 1550, and Si IV $\lambda\lambda$1393, 1402 lines. The C IV doublet appears saturated. All the lines in this system agree within $\Delta z \lesssim 0.0001$.

$z_{abs} = 2.01623$.—This is the weaker system of the complex and was probably blended with the $z_{abs} = 2.01378$ system in the data of S87. The ratio of the C IV doublet is 1.59 ± 0.02 and the redshift agreement is $\Delta z = 0.00001$. There is no evidence for the Si IV doublet in this system.

$z_{abs} \simeq 2.07660$.—The C IV doublet of this system remains broad and troughlike, and the components of the doublet unresolved in our high-resolution data. This system was identified by S87 as having three components based on structure in the lines they identified as Si IV. We believe the sharp features identified by S87 as Si IV $\lambda\lambda$1393, 1402 are actually C IV doublets superposed on the smooth unresolved Si IV doublet belonging to this system. We identified the sharp features as members of three new systems: $z_{abs} = 1.75530$, 1.77668 and 1.77764. The FWHM of the unresolved Si IV and C IV doublets are $\sim$2400 km s^{-1} and $\sim$1600 km s^{-1}, respectively. There is evidence for a broad depression where we would expect to see N V $\lambda\lambda$1238, 1242, but the spectrum does not extend sufficiently blueward to cover the entire feature. Because the Si IV and C IV doublets are unresolved, the redshift of this system is highly uncertain.

$z_{abs} = 2.14674$.—This certain system consists of a broad, shallow C IV doublet and Si II 1526 line. There are associated broad, shallow features at the location where N V $\lambda\lambda$1238, 1242, and Lyα are expected. There is also evidence in our data for the two sharp features in the C IV complex noted by S87. The features show good redshift agreement and are in the correct ratios for identification as C IV at $z_{abs} = 2.1455$. Higher resolution data is required to resolve this complex. The redshift of this system $z_{abs} = 2.14674 \pm 0.00005$ is based on the weighted average redshift of the Si II and C IV lines.

4.3. *Tololo 1035−2737*

The spectrum of Tol 1035−2737 is shown in Figure 4. This QSO (number 16 of the Bohuski & Weedman 1979 list) is located roughly 40′ southwest of Tol 1037−2704 and Tol 1038−2712 (Fig. 1), corresponding to a projected distance of ∼10 Mpc. From the peaks of the emission lines, we measured the redshift to be $z_{em} = 2.159 \pm 0.014$, in good agreement with the redshift determined by S87 and J88. At this redshift the QSO lies behind all the common systems seen in the original pair, and is possibly a cluster member situated at the far side of the proposed supercluster. S87, in a footnote added in proof, reported a definite C IV absorption system at $z_{abs} = 2.125$ and two possible systems at $z_{abs} = 2.040$ and $z_{abs} = 1.905$ from a slit spectrum with 4 Å resolution. J88 observed this QSO at 6 Å resolution; they verified the system at $z_{abs} \simeq 2.125$ and identified only one other system at $z_{abs} = 1.982$. These C IV systems coincide with some systems in the original Tololo pair within a velocity separation less than 5000 km s^{-1}. This makes this QSO particularly important for further study.

$z_{abs} = 0.82381$.—This is a certain system, based on the presence of the strong Mg II λλ2796, 2803 doublet and Fe II λλ2344, 2382, 2586, 2600. The ordering of the line strengths correspond well with expectation, except for the Fe II λ2586 line, which appears to be blended with another (unidentified) line.

$z_{abs} = 0.82467$.—As above, this system is certain, based on the presence of a saturated Mg II doublet and Fe II lines. There is evidence for the Fe II λ2374 line, but its equivalent width falls below the 5 σ threshold for detection. Fe II λ2382 may be blended with Fe II λ1608 from the $z_{abs} = 1.70313$ system.

$z_{abs} = 1.70313$.—The identification of this system is primarily based on the presence of a strong C IV doublet, with both members at $z_{abs} = 1.70313 \pm 0.00001$ and a doublet ratio of DR = 1.54 ± 0.06.

$z_{abs} = 1.73058$.—This system is identified solely by the presence of a strong C IV doublet. Both lines agree to within $\Delta z \lesssim 0.00003$.

$z_{abs} = 1.84089$.—This system is based on the presence of C IV λλ1548, 1550. The redshift agreement between the doublet members is $\Delta z \lesssim 0.00001$. We identify no other lines associated with this system.

$z_{abs} = 1.92965$.—The identification of this system is based solely on the weak C IV doublet. Both members agree within $\Delta z \lesssim 0.00003$ and doublet ratio is ∼2.

$z_{abs} = 2.12630$.—The identification of this system is based on the presence of the C IV doublet and N V λλ1238, 1242. There is some evidence in the N V lines that the system will split into two components in higher resolution data.

4.4. *Tololo 1029−2654*

The spectrum of Tol 1029−2654 is shown in Figure 5. This QSO was discovered in our own survey for nearby QSOs in a 2°.5 × 3° field centered on the original QSO pair using an objective prism plate from the UK Schmidt Telescope. It is situated about 99′ or 24 Mpc northwest of Tol 1037−2704 and roughly 115′ or 28 Mpc northwest of Tol 1038−2712 (Fig. 1). We estimated $z_{em} = 2.586 \pm 0.018$ from the peaks of the Lyα and Si IV emission lines. An obvious feature in the spectrum of Tol 1029−2654 is the presence of a damped Lyman-α system at the redshift $z_{abs} = 2.549$. We observe Si II λλ1190, 1193, Si II λ1260, O I λ1302, Si II λ1304, C II λ1334 and Si II λλ1393, 1402 associated with this damped Lyman-α system. We are not aware of any previously published spectra of this QSO.

$z_{abs} = 2.01744$.—This probable system is identified by a relatively weak C IV doublet, with both members at $z_{abs} = 2.01744 \pm 0.00001$ and a doublet ratio of DR = 1.52 ± 0.04.

$z_{abs} = 2.01840$.—This is another probable system with a weak C IV doublet. Both lines agree to within $\Delta z \lesssim 0.00001$.

We base our decomposition of the following complex into four systems primarily on the structure in the C IV lines.

$z_{abs} = 2.02549$.—This strong system is certain. In addition to the C IV doublet, we tentatively identify the Si IV doublet although Si IV λ1402 is probably blended with another line in the Lyα forest.

$z_{abs} = 2.02617$.—The strong C IV doublet is severely blended with the system at $z_{abs} = 2.0268$, but is no doubt real. The redshift agreement between the doublet members is $\Delta z \lesssim 0.00001$. No other lines are observed.

$z_{abs} = 2.02662$.—This system is the most certain, consisting of the saturated C IV doublet, the Si IV doublet and possibly the C II λ1334 line. The redshift agreement between the doublets of C IV and Si IV is better than 0.00003, whereas there is a significant discrepancy in redshift between the doublets and the line identified as C II λ1334.

$z_{abs} = 2.02716$.—This is the weakest component of this complex. It is severely blended with the C IV lines of the $z_{abs} = 2.0268$ system, but is most probably real.

5. CHARACTERISTICS OF THE C IV ABSORPTIONS SYSTEMS

Table 7 lists the 47 C IV systems found in the spectra of the four Tololo QSOs. The columns of Table 7 list the minimum (col. [1]) and maximum (col. [2]) redshifts between which a C IV doublet could have been detected, the weighted mean absorption redshift (col. [3]) of the C IV system and its associated uncertainty (col. [4]), and the number of lines on which we based the identification (col. [5]). Only the lines that were certain to belong to the system and those that were not blended were used to calculate the mean redshift. Column (6) gives the difference between the absorption redshift of the system and the emission redshift of the QSO in terms of the fraction β of the velocity of light defined as

$$\beta = \frac{(1 + z_{em})^2 - (1 + z_{abs})^2}{(1 + z_{em})^2 + (1 + z_{abs})^2} . \quad (1)$$

Columns (7) and (8) list the rest equivalent widths of the components of the C IV doublet. Column (9) classifies the reliability of the identifications as either certain, probable or possible. A system was considered certain if it contained lines in addition to the C IV doublet; probable if only the doublet was identified, but both lines were present at the 5 σ level and the velocity match and ratio of the lines was good; and possible if either only one line of the C IV doublet was observed at 5 σ level, but the other line was present at a lower level (>3 σ), or there was any ambiguity in the line identification.

In order to judge the reliability of the C IV systems whose identifications were based solely on the doublet, we compared the doublet ratios DR = $W_0(1548)/W_0(1550)$ and rms velocity difference between the doublet components for both the certain and probable systems. The DR and velocity difference distributions, constructed using C IV doublets that are not blended, are shown in Figure 6 and 7, respectively. The DR histogram of certain systems shows more doublets with ratios of unity than that of the probable systems. This is not unexpected and is due to the fact that the certain systems (defined as those that contain lines other than the C IV doublet) are more likely to

TABLE 7

C IV ABSORPTION SYSTEMS

z_{min} (1)	z_{max} (2)	z_{abs} (3)	$\sigma(z_{abs})$ (4)	Number (5)	β (6)	$W_0(1548)$ (7)	$W_0(1550)$ (8)	Reliability (9)
				Tol 1037–2704; $z_{em} = 2.193$				
1.46	2.19	1.48248	0.00001	2	0.2465	0.24	0.19	probable
		1.48323	0.00001	2	0.2462	0.16	0.12	probable
		1.63336	0.00001	2	0.1904	0.11	0.05	probable
		1.63434	0.00001	2	0.1900	0.55	0.50	probable
		1.91249	0.00001	7	0.0917	0.26	0.22	certain
		1.97145	0.00002	4	0.0718	0.16	0.13	certain
		1.97216	0.00001	6	0.0716	0.34	0.23	certain
		2.00336	0.00002	2	0.0612	0.09	0.07	probable
		2.02509	0.00001	2	0.0540	0.07	0.04	probable
		2.02785	0.00001	5	0.0531	0.32	0.29	certain
		2.02847	0.00001	5	0.0529	0.22	0.15	certain
		2.03915	0.00003	1	0.0493	0.06	...	possible
		2.07059	0.00002	4	0.0391	0.54	0.47	certain
		2.07716	0.00003	4	0.0369	0.22	0.11[a]	probable
		2.07858	0.00003	4	0.0365	0.40	0.20[a]	certain
		2.08321	0.00003	4	0.0350	2.15[b]	1.22	certain
		2.10663	0.00001	2	0.0274	0.06	0.04	probable
		2.11561	0.00001	2	0.0245	0.05	0.04	probable
		2.12818	0.00001	6	0.0205	0.58	0.47	certain
		2.13593	0.00001	7	0.0180	0.70	0.57	certain
		2.13910	0.00001	10	0.0170	0.75	0.68	certain
		2.14030	0.00002	9	0.0166	0.20	0.17	certain
		2.14239	0.00001	4	0.0160	0.07	0.03	certain
				Tol 1038–2712; $z_{em} = 2.331$				
1.46	2.31	1.75530	0.00002	2	0.1875	0.09	0.09	probable
		1.77688	0.00003	2	0.1800	0.09	0.09	probable
		1.77764	0.00003	2	0.1797	0.18	0.16	probable
		1.85055	0.00002	2	0.1545	0.07	...	possible
		1.89309	0.00003	1	0.1400	0.04	...	possible
		1.89353	0.00002	2	0.1399	0.05	0.04	probable
		1.95490	0.00001	5	0.1192	0.29	0.21	certain
		1.95610	0.00001	3	0.1188	0.04	0.02	certain
		1.96047	0.00001	4	0.1174	0.17	0.12	certain
		2.01378	0.00001	4	0.0997	0.79	0.63	certain
		2.01623	0.00001	2	0.0989	0.09	0.06	probable
		2.07660	0.00011	4	0.0793	1.87[c]	1.87[c]	certain
		2.14674	0.00005	5	0.0568	0.42	0.40	certain
				Tol 1035–2737; $z_{em} = 2.149$				
1.46	2.15	1.70313	0.00001	2	0.1515	0.23	0.16	probable
		1.73058	0.00001	2	0.1416	0.26	0.16	probable
		1.84089	0.00001	2	0.1026	0.15	0.08	probable
		1.92965	0.00002	2	0.0721	0.09	0.04	probable
		2.12631	0.00001	4	0.0072	0.19	0.13	certain
				Tol 1029–2654; $z_{em} = 2.586$				
1.82	2.31	2.01744	0.00002	2	0.1709	0.11	0.07	probable
		2.01840	0.00002	2	0.1706	0.13	0.10	probable
		2.02543	0.00001	4	0.1684	0.23	0.19	certain
		2.02616	0.00001	2	0.1681	0.14	0.10	probable
		2.02660	0.00001	5	0.1680	0.29	0.27	certain
		2.02716	0.00001	2	0.1678	0.06	0.02	probable

[a] The C IV λ1550 component is blended with the C IV λ1548 line of the $z_{abs} = 2.08301$ system. It has been assigned an equivalent corresponding to half that of the unblended C IV λ1548.

[b] C IV λ1548 is blended with the C IV λ1550 lines of the $z_{abs} = 2.07741$ and 2.07820 systems. It has been assigned the measured equivalent width of the blended C IV λ1548 minus the contributions by C IV λ1550.

[c] The C IV $\lambda\lambda$1548, 1550 doublet is not resolved. Each component has been assigned half the equivalent width of the doublet.

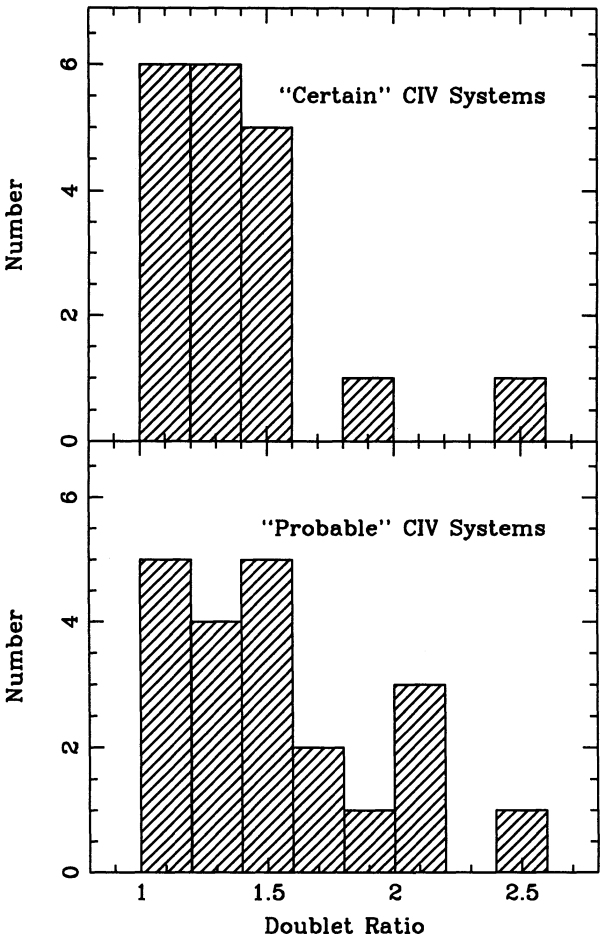

FIG. 6.—Histograms of C IV doublet ratios DR = $W_0(1548)/W_0(1550)$ for the certain (*upper panel*) and probable (*lower panel*) systems.

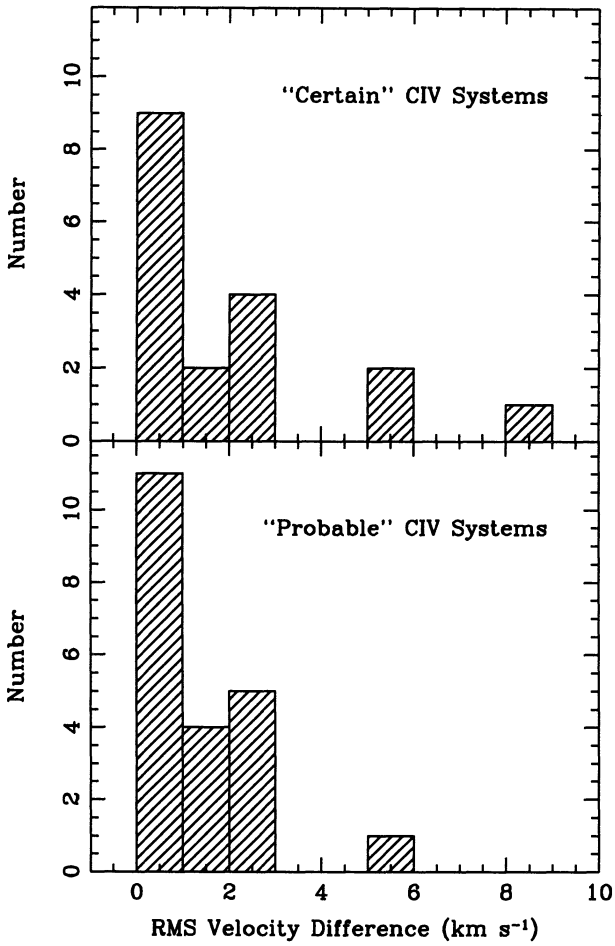

FIG. 7.—Histograms of rms velocity differences between C IV doublet components for the certain (*upper panel*) and probable (*lower panel*) systems.

have strong and saturated C IV lines. We find a mean value of $\langle DR \rangle = 1.35$ and standard deviation $\sigma(DR) = 0.33$ for the certain systems, consistent with the values found by Young et al. (1982) in a sample of 30 QSOs. A χ^2-test indicated that no significant difference exists between the doublet ratio and velocity difference distributions of the certain and probable systems. Similarly, a χ^2-test confirmed that the distribution of velocity differences of the probable systems is consistent with that of the certain systems.

We have defined four samples of C IV systems in Table 8. The largest sample S1 contains the 44 certain and probable systems listed in Table 7. S2 is a subset of sample S1 with all possible associated systems within $\beta c \leq 5000$ km s^{-1} of the emission redshift of the QSO excluded (see, e.g., Foltz et al. 1986). The third sample S3 contains 21 lines for which the rest equivalent widths of both components in a given C IV doublet exceed 0.15 Å. This sample is most readily comparable to the sample A4 of SBS. In S4, complexes with component separation $\Delta v \leq 1000$ km s^{-1} have been collapsed into single systems.

The distribution of rest equivalent widths for C IV absorption lines has been found to be well fitted by an exponential function of the form

$$n(W) = \left(\frac{N_*}{W_*}\right) e^{-W/W_*}, \qquad (2)$$

where $n(W) = \partial^2 N/\partial z\, \partial W$ is the density of lines per unit ΔW and Δz. Following SBS, we approximated $n(W)$ by counting the number of lines in bins of width ΔW such that $n(W) \simeq \Delta N/\Delta z\, \Delta W$, where Δz is the total range of redshifts of the sample QSOs.

TABLE 8

C IV ABSORPTION SYSTEM SAMPLES

Criteria	Sample	#	$< z_{abs} >$	W_*	$\sigma(W_*)$	N_*	$\sigma(N_*)$
All definite & probable systems	S1	44	1.958	0.33	0.04	77	22
$\beta c > 5000$ km s^{-1}	S2	41	1.947	0.33	0.04	73	20
$\beta c > 5000$ km s^{-1}, $W_0 > 0.15$ Å	S3	21	1.961	0.39	0.04	53	11
$\beta c > 5000$ km s^{-1}, $W_0 > 0.15$ Å, $\Delta v > 1000$ km s^{-1}	S4	16	1.937	0.41	0.06	40	13

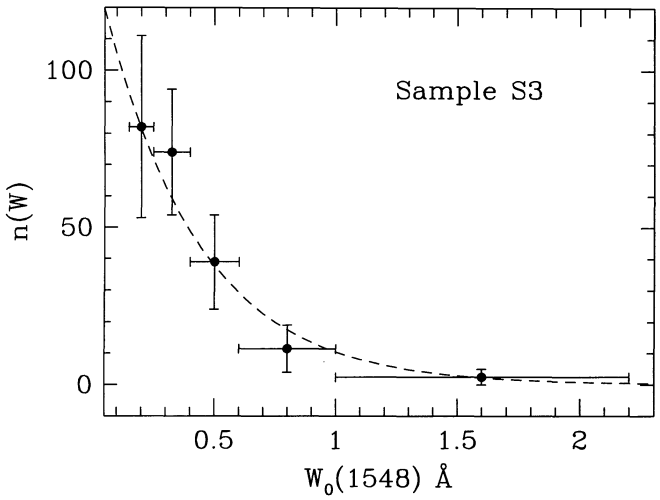

FIG. 8.—Distribution of rest equivalent widths for sample S3. The vertical error bars give the estimated uncertainty in each bin, and the horizontal bars represent ΔW. The dashed curve gives the best fit for an exponential function of the form $n(W) = (N_*/W_*) \exp(-W/W_*)$, where $W_* = 0.39 \pm 0.04$ and $N_* = 53 \pm 11$.

The binned equivalent width distribution is plotted in Figure 8 for sample S3 ($W_0 > 0.15$ Å and $\beta c > 5000$ km s^{-1}). The vertical error bars give the estimated uncertainty in each bin, and the horizontal bars represent ΔW. The best fit to the equivalent width distribution is an the exponential curve with $W_* = 0.39 \pm 0.04$. Our results agree with SBS, who found for their sample A4 ($W_0 > 0.15$ Å), $W_* = 0.46 \pm 0.04$. In order to investigate the trend in the equivalent width distribution for weaker lines ($W_0 < 0.15$ Å), we have plotted in Figure 9 the equivalent width distribution for sample S1. It is clear from this plot that a single exponential function is not a good representation of the equivalent width distribution over the entire range of W_0 due to the steep increase in line density for $W_0 <$ 0.3 Å. This feature of the distribution is also consistent with the results of SBS. The best-fit values of W_* and N_* for samples S1 through S4 are given in Table 8. Thus we are confident that the C IV absorption systems toward the Tololo QSOs are consistent with, and belong to, the same population of absorbers as the SBS systems.

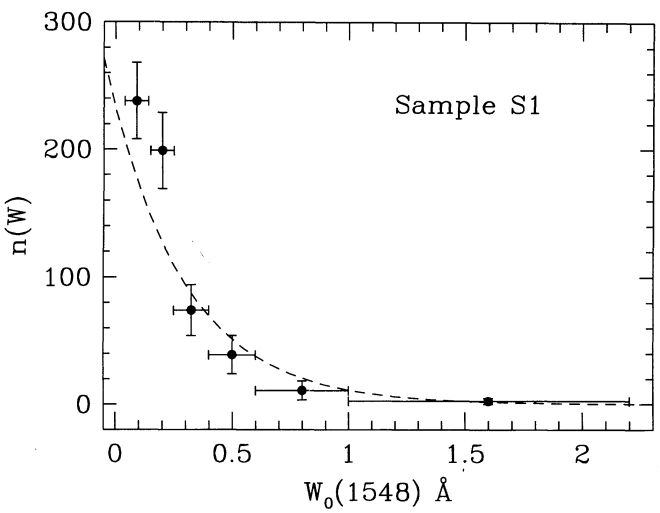

FIG. 9.—Same as Fig. 8 for sample S1. The dashed curve is the best fit for an exponential function where $W_* = 0.33 \pm 0.04$ and $N_* = 77 \pm 11$.

6. THE VELOCITY AND SPATIAL CORRELATION FUNCTIONS

The fact that the C IV absorbers are thought to be associated with either galaxies or their precursors makes it of interest to examine the clustering properties of the C IV systems in our sample. There is considerable evidence that the C IV absorbers are clustered on velocity scales out to $\Delta v \simeq 10{,}000$ kms (SBS; HHW). Also, the spatial correlation function of Crotts (1985) appears to show marginal evidence (95% significance level) for clustering on comoving separations of $\lesssim 2$ Mpc. Our high-resolution spectra allow us to examine the clustering properties of the C IV absorbers on smaller velocity scales (down to $\Delta v \simeq 30$ km s^{-1}) along the lines of sight to the QSOs and spatially on scales out to $r \simeq 440$ Mpc.

To measure the degree and scale to which the C IV systems cluster spatially and in redshift toward the QSOs, we have computed the two-point correlation function, $\xi(r)$, which is defined such that the probability of finding an absorber at distance r from another in a volume element dV is

$$dP = n[1 + \xi(r)]dV \,, \tag{3}$$

where n is the average number density of absorbers. The correlation amplitude is defined explicitly by the expression

$$\xi(r) = \frac{N_{\rm obs}}{N_{\rm exp}} - 1 \,, \tag{4}$$

where $N_{\rm obs}$ is the observed number of line pairs with separations between r and $r + \Delta r$, and $N_{\rm exp}$ is the number of pairs expected for a random distribution of absorbers. For $\xi(r) > 0$, the correlation function measures the *additional* probability over the background of finding an absorber at a distance r from a randomly placed absorber. An identical equation holds for the velocity correlation function, $\xi(v)$.

The usual expression for the variance $\sigma^2 = N_{\rm exp}^{-1}$ in $\xi(r)$ is an underestimate of the true error because the pair count, $N_{\rm exp}$, is not a Poisson variable even if the redshifts are distributed randomly (Olivier et al. 1993). Therefore, we computed the variance in $\xi(r)$ from the equation

$$\sigma^2(\xi) = \sigma^2(N_{\rm obs})\left(\frac{1}{\langle N_{\rm exp}\rangle}\right)^2 = \frac{\langle N_{\rm obs}^2\rangle - \langle N_{\rm obs}\rangle^2}{\langle N_{\rm exp}\rangle^2} \,, \tag{5}$$

where $\langle N_{\rm obs}^2\rangle$, $\langle N_{\rm obs}\rangle$, and $\langle N_{\rm exp}\rangle$ were estimated numerically from 1000 Monte Carlo realizations of randomly distributed absorbers in the same redshift range as the data sample and with the same number of redshift systems. The uncertainty calculated in this manner measures the probability that a random distribution of redshifts could lead to the measured value of $\xi(r)$ in a given bin along the identical four lines of sight containing the same number of redshift systems as observed in the sample. Although this is a better measure of the uncertainty per bin, it is still an underestimate where $\xi(r) \gtrsim 1$.

6.1. *The Velocity Correlation Function*

We estimated the velocity correlation function $\xi(v)$ using the method described in detail in HHW. First, we decided on a set of bins such that the average occupancy based on randomly distributed absorbers was the same in each bin, giving equal sensitivity to departures from a Poisson distribution. Then, we estimated the number of observed pairs in each bin by computing, for each C IV system, the redshift intervals whose velocity

separations with respect to that system corresponded to the given bin. We checked that the redshift intervals resided within the redshift range spanned by the data, and, if necessary, adjusted the size of intervals such that they did. Finally, we counted the number of systems in the *same* line of sight that fell within the redshift intervals to get an estimate of the number of observed pairs.

We estimated the number of expected pairs using the catalogs of C IV systems in SBS and Steidel (1990). We first calculated the number density of systems per unit redshift by counting the number of systems in the catalog lines of sight that fell within larger ($\pm 25{,}000$ km s^{-1}) redshift intervals centered on the small intervals, and dividing this by the total path length intersected by the large intervals for which C IV systems could have been found in the catalog QSOs. Bins of width $\pm 25{,}000$ km s^{-1} were adopted since the velocity correlation function shows no evidence of clustering on scales greater than $\sim 10{,}000$ km s^{-1} (SBS; Steidel 1990; HHW). We then obtained the number of expected pairs by multiplying the average number density of systems by the redshift intervals in which the number of observed pairs was derived.

This procedure was repeated treating each redshift system as the reference system and accumulating the numbers of observed and random pairs in each bin. The method automatically takes into account the nonuniform wavelength coverage of the data sample without having to make an explicit correction. Furthermore, it is designed to be independent of any assumptions about the evolution in absorber population. The velocity separation between absorbers was calculated using the approximation $\Delta v \simeq c\,\Delta z/(1+\bar{z})$, where $\Delta z = z_2 - z_1$ and $\bar{z} = \frac{1}{2}(z_1 + z_2)$. We verified our calculations by successfully reproducing the results of HHW. We also generated random data sets, placing systems over the same redshift ranges covered by the QSO data, and verified that $\xi(v)$ scattered about zero as expected for a random distribution of absorbers.

Our calculation of $\xi(v)$ deviates from that of HHW in one important way. HHW used the same sample of redshifts to calculate both the observed and expected number of pairs. It would not be appropriate in our case to do the same because the lines of sight are not typical, having been selected for a detailed study from a priori knowledge of their abnormally complex absorption spectra. We modified their procedure to use a sample of C IV absorbers found along the lines of sight to randomly selected QSOs to estimate the expected number of pairs. The sample was a combination of two homogeneous and complementary surveys for C IV systems described in SBS and Steidel (1990). Together the surveys found 275 C IV absorption systems in the spectra of 66 QSOs, with a sensitivity designed to detect all systems with rest equivalent widths exceeding 0.15 Å. We restricted our attention to a subsample of 138 systems satisfying the criteria $W_0 > 0.15$ Å in both C IV lines and $\beta c > 5000$ km s^{-1}. This subsample contains absorbers with redshifts ranging from $1.2 \lesssim z_{\rm abs} \lesssim 3.6$ and median $z_{\rm abs} = 2.015$.

One disadvantage in using the SBS sample to estimate the number of expected pairs arises because our data were obtained at higher resolution than the data of SBS. This introduces uncertainty into the normalization of the correlation function. It is well known that the number of C IV systems detected depends on the spectral resolution, since many systems break up into narrower components in higher resolution data (Blades 1988). Therefore, it was necessary to normalize the observed correlation function by the mean over-density $\bar{\varrho}$ of systems. We estimated $\bar{\varrho}$ numerically from the average ξ of 1000 Monte Carlo realizations of randomly distributed absorbers in the same redshift sensitivity intervals and with the same number of systems as in the relevant data sample. As expected, the correlation function is flat for an unclustered sample and the standard deviation of the amplitude among the bins implies an uncertainty in the normalization of $\lesssim 10\%$.

The velocity correlation function of the 44 C IV systems in sample S2 is shown in Figure 10 normalized by $\bar{\varrho} = 6.7$. The error bars are the 1 σ statistical errors for a random distribution of absorbers. There are five features of note in Figure 10: (1) The strongest correlations appear in the smallest velocity bin with $\Delta v \leq 300$ km s^{-1}. These correlations are thought to be predominantly due to the motions of individual clouds in galactic halos since the typical velocity dispersions of the clouds are about 200–300 km s^{-1} (Davis & Peebles 1983). (2) We also detect strong signal in the second bin for velocity separations in the range $300 \leq \Delta v \leq 1000$ km s^{-1}, which corresponds to the velocity dispersions of typical galaxy clusters ($\sigma_v \simeq 300-1400$ km s^{-1}; Zabludoff et al. 1993). (3) The correlation signal appears to persist out to velocity separations of $\Delta v \lesssim 13{,}000$ km s^{-1}, though the power in the velocity bin $10{,}000 \leq \Delta v \leq 13{,}000$ km s^{-1} is most likely an artifact of the subsplitting of the C IV complexes. We explore this point in more detail below. (4) On velocity scales of $20{,}000 \leq \Delta v \leq 35{,}000$ km s^{-1}, there is an apparent 2.8 σ deficit of correlation signal, also discussed in more detail below. (5) Finally, in the bins corresponding to $\Delta v \geq 35{,}000$ km s^{-1}, we find $\xi(v) \simeq 0$, consistent with no clustering of the absorbers.

Most of the power in Figure 10 appears to be confined to well-defined peaks. We investigated the possibility that this is an artifact of the adopted bin boundaries by experimenting with different bin sizes and shifting the centers of the bins. We found that regardless of the location of the bin boundaries, the structure in $\xi(v)$ persisted. Upon close examination of the data, this is not so surprising. Figure 11 shows the redshift distribution of C IV systems in the Tololo QSOs. The systems are clearly clustered in five complexes in Tol 1037−2704 and Tol 1038−2712 with roughly equal spacing [though the $z_{\rm abs} = 1.85055$ system in Tol 1038−2712 was classified as a possible system and therefore was not included in the calculation of the $\xi(v)$]. This feature has been pointed out by J86 and S87. The spacing between each cluster of systems is approximately 5000–7000 km s^{-1}, which is consistent with the separation between the peaks in the redshift correlation function. The most likely cause of the pattern of peaks is beating between the five clusters of systems, where the third and fourth peaks represent higher harmonics. Similarly, the deficit in the correlation function between $20{,}000 \leq \Delta v \leq 35{,}000$ km s^{-1} is caused by beating between the two clusters of systems at $z_{\rm abs} \simeq 1.48$ and 1.63 and the five clusters of system at the opposite end of the accessible redshift range between $z_{\rm abs} \simeq 1.91$ and 2.14 in Tol 1037 − 2704 (Fig. 11).

In order to eliminate the beating effects in $\xi(v)$, we collapsed complexes with component separations $\Delta v \leq 1000$ km s^{-1}, consistent with the typical line-of-sight velocity dispersions of clusters of galaxies (Zabduloff et al. 1993, Fig. 4), into single systems. The velocity correlation function was then recalculated for the remaining 16 C IV systems with $W_0 > 15$ Å (sample S4), and is shown, normalized by $\bar{\varrho} = 2.1$, in Figure 12*a*. As expected, there is no correlation signal corresponding to clusters of galaxies. However, significant signal persists for

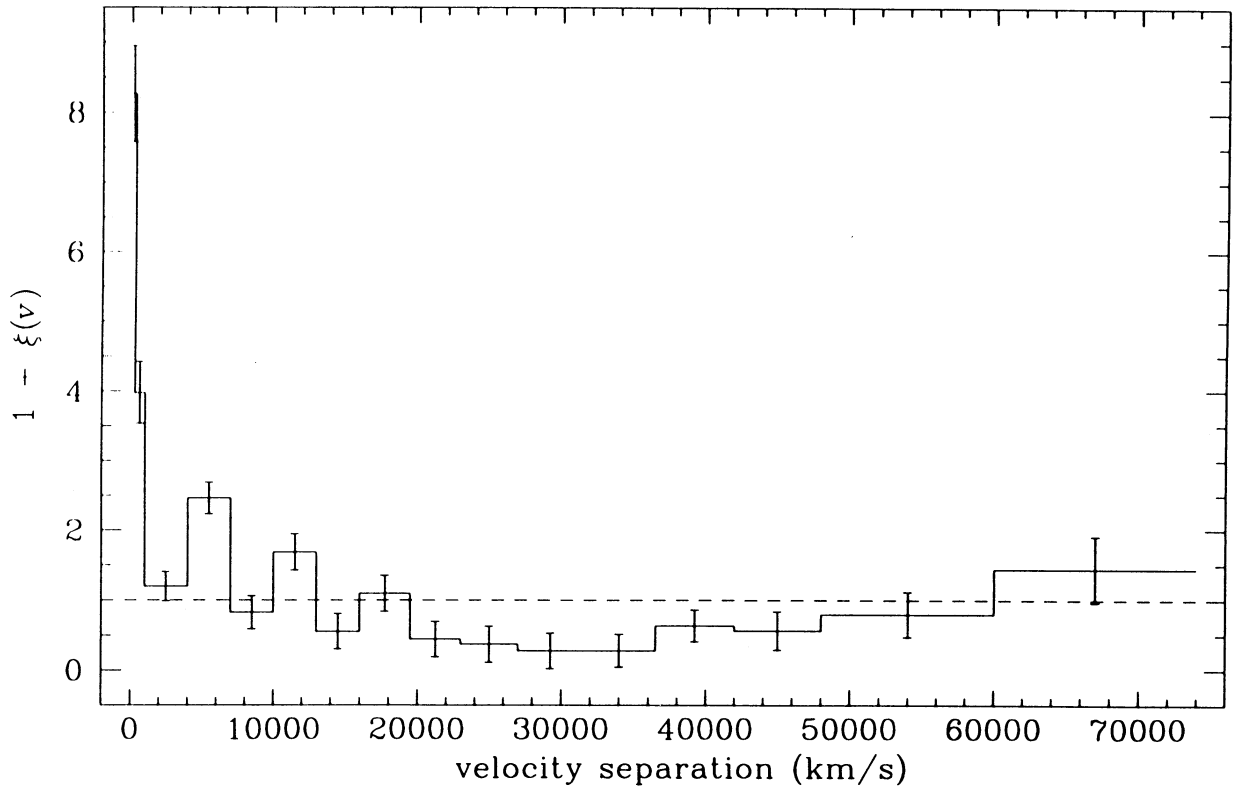

FIG. 10.—Two-point velocity correlation function for the 44 C IV absorbers in sample S2. Error bars represent 1 σ uncertainties for a random distribution of absorbers.

velocity separations of $4000 \leq \Delta v \leq 7000$ km s^{-1}. We simulated this effect by placing systems with velocity separations of 5500 ± 1000 km s^{-1} in the redshift range $1.80 \leq z \leq 2.15$. We also required that some of the absorbers in the line of sight to Tol 1037−2704 have redshifts $z_{abs} = 1.45$ and 1.65 in order to simulate the apparent deficit of signal in the largest velocity bins. The result of the simulations is shown in Figure 12*b* and shows excellent agreement with the observed correlation function. The peak in the velocity splitting histogram corresponds to a comoving spatial scale of ~ 30–$40\ h^{-1}$ Mpc. Since the power associated with virialized clusters on smaller scales has been removed, we can be confident that this highly significant (4.3 σ) peak represents power on supercluster scales.

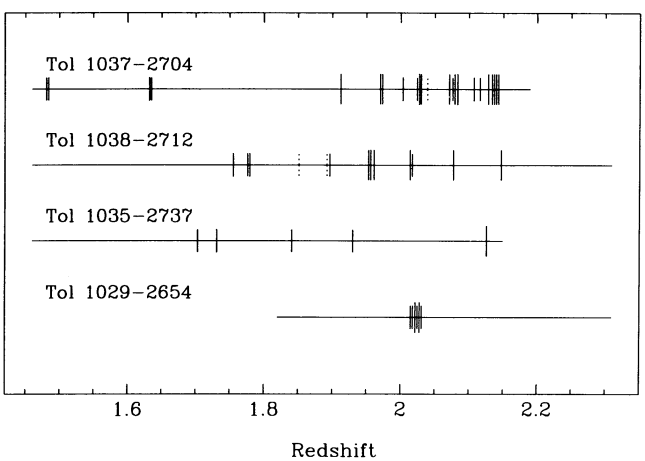

FIG. 11.—Redshift distribution of C IV systems toward the lines of sight to the four QSOs. The long vertical lines represent the certain systems, and the short lines represent the probable systems. The possible systems are indicated by dotted lines. Some of the closely spaced systems have been shifted slightly to distinguish them in the plot.

For small velocity separations, there is no easy way to relate the velocity correlation function to the spatial correlation function derived from three-dimensional surveys without some knowledge of the internal structure, kinematics, and small-scale clustering properties of the absorbers (HHW). However, for large velocity separations, the relationship between the correlation functions is straightforward. Adopting the model of HHW, the velocity correlation function resembles a Gaussian of width σ at small velocities and tails off as a power law at large velocities. Based on observations of nearby galaxies and clusters, it is reasonable to assume $\sigma \simeq 3$ km s^{-1}. For separations greater than 3 σ ($\simeq 900$ km s^{-1}), the contribution to $\xi(v)$ from the Gaussian component becomes negligible and $\xi(v)$ is dominated by the power-law component. Therefore, for velocity differences exceeding 1000 km s^{-1}, it is possible to compare $\xi(r)$ directly with $\xi(v)$.

The amplitude of the correlations is estimated to be 2.35 ± 0.55 in the velocity bin $4000 \leq \Delta v \leq 7000$ km s^{-1}, where most of the power exists (Fig. 12). This value was determined from the two-point correlation function for the S4 sample where velocity separations on scales less than 1000 km s^{-1} have been removed. This ensures that the correlation function on large scales is uncontaminated by "beating" effects and allows direct comparison with the spatial correlation function of clusters of galaxies.

The two-point autocorrelation function $\xi_{cc}(r)$ of 351 Abell clusters for richness classes RC = 0 and RC > 1 is well

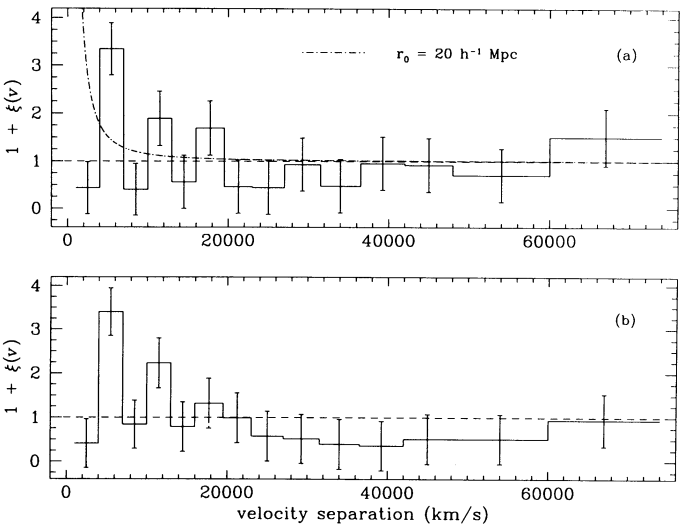

FIG. 12.—(*a*) Two-point velocity correlation function for the 16 C IV absorbers in sample S4. $\xi(v)$ is 2.35 ± 0.55 in the bin corresponding to the velocity separations of $4000 < v < 7000$ km s^{-1}. For $v > 7000$ km s^{-1}, $\xi(v)$ is consistent with no clustering signal. The dot-dashed curve represents the spatial correlation function for rich clusters of galaxies, which is well described by a power law $(r/r_0)^{-1.8}$, where $r_0 = 20\ h^{-1}$ Mpc. (*b*) Same as (*a*) for simulated samples of absorbers.

described between $r = 10$ and $70\ h^{-1}$ Mpc by a power law $(r/r_0)^{-1.8}$, where $r_0 = 20(\pm 4.3)\ h^{-1}$ Mpc (Postman, Huchra, & Geller 1992). We have superposed this relation, assuming a correlation length $r_0 = 20\ h^{-1}$ Mpc, onto the correlation function derived in Figure 12*a*. The amplitude of the correlation function toward the Tololo QSOs at comoving scales of ~ 30–$40\ h^{-1}$ Mpc is clearly significantly larger than $\xi_{cc}(r)$ for even the richest (RC > 1) clusters of galaxies.

6.2. *Spatial Correlation Function*

The spatial correlation function $\xi(r)$ was determined in the same manner as the velocity correlation function, but this time pairing systems along *different* lines of sight in order to obtain a measure of the true spatial clustering. Again we decided on a set of bins such that the average number of expected pairs based on randomly distributed absorbers was roughly the same in each bin. This time the bin sizes varied nonuniformly as a function of comoving separation since there is a tendency for the number of observed pairs to accumulate near the perpendicular separations of neighboring lines of sight. To estimate number of observed pairs in each bin, we treated each redshift system along a given line of sight in turn as a reference system and calculated the redshift intervals in each of the neighboring lines of sight that corresponded to the comoving separation represented by that bin. We then checked that the intervals fell within the redshift range sampled by the data, and counted the number of redshift systems that fell in the respective intervals to get the number of observed pairs.

The number of expected pairs was determined using the same catalog of C IV absorption systems used to estimate the redshift correlation function. Intervals of size ± 200 Mpc were used to estimate the number density of systems per unit redshift since no clustering is evident on spatial scales greater than about 150 Mpc (Bahcall & Soneira 1983). We found the centers of the bins in which the number of observed pairs was determined and calculated the redshift intervals with respect to those centers in each of the neighboring lines of sight that corresponded to the comoving separation of the larger (± 200 Mpc) intervals. We then adjusted the intervals so that they fell within the redshift range spanned by the data of the catalog QSOs, and counted the number of redshift systems in each catalog line of sight that fell within the larger intervals. This is equivalent to setting each of the catalog QSOs at the angular separations of the Tololo QSOs. Finally, in a manner analogous to the redshift correlation function, we derived the average number of redshift systems per unit redshift by dividing the total number of redshift systems by the total path length spanned by the large bins in which a C IV system would have been detected. We then multiplied this average number density of systems by the small redshift intervals to get the number of expected pairs in that bin.

As before, we assumed $q_0 = 0.5$. This simplified the computations, since the spatial separation of any two absorbers is given by the familiar Euclidean law of cosines, $r_{12} = (r_1^2 + r_2^2 - 2r_1 r_2 \cos \alpha)^{1/2}$, where α is the angular separation of the neighboring lines of sight and $r_{1,2} = (2c/H_0)[1 - (z_{1,2} + 1)^{-1/2}]$ is the comoving distance to the absorbers. We restricted the range of study to $12 \leq r \leq 440$ Mpc, where the lower limit corresponds to the perpendicular separation of the closest pair of QSOs.

The resultant spatial correlation function $\xi(r)$ is shown normalized by $\bar{\varrho} = 2.0$ in Figure 13 for sample S4, which contains no correlation signal from clusters of galaxies (see § 6.1.). The error bars are the 1 σ statistical errors for a Poisson distribution of redshifts (eq. 5). There is no convincing evidence for any spatial correlation signal over scales from $18 \leq r \leq 440\ h^{-1}$ Mpc. However, a signal of the same amplitude and scale as the velocity correlation function (Fig. 12), is present in the smallest bin $r < 18\ h^{-1}$ Mpc, although in this case the error bars are larger because of the sparse sampling of this pencil beam experiment. All of the correlation signal in this bin is derived from the systems belonging to the two closest QSOs, Tol 1037−2704 and Tol 1038−2712; the separations of the other two QSOs are too large to make any contribution on comoving scales less than $\sim 30\ h^{-1}$ Mpc. We estimate the amplitude of the correlations to be $\xi(r) = 2.7 \pm 1.2$ between comoving separations $12 < r < 18\ h^{-1}$ Mpc. In order to test whether the signal in this bin is caused primarily by the high density of systems toward Tol 1037−2704 and Tol 1038−2712, we performed Monte Carlo simulations with random data sets keeping the number of systems along each line of sight fixed. In 1000 trials, the measured signal, $\xi(r) = 2.7$,

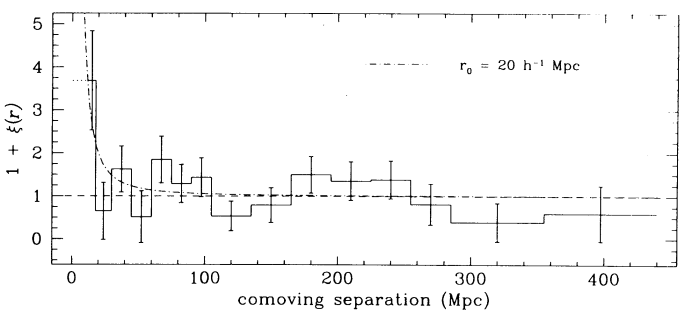

FIG. 13.—Two-point spatial correlation function for the 16 C IV absorbers in sample S4. The error bars represent the 1 σ uncertainties. $\xi(r)$ is 2.7 ± 1.2 in the lowest bin ($r < 18$ Mpc), corresponding a marginally significant detection of 2.1 σ, and is consistent with zero everywhere else. The dot-dashed curve represents the power-law relation of the spatial correlation function for rich clusters of galaxies.

was exceeded 32 times, implying a slightly lower significance (2.1 σ) than inferred by its estimated uncertainty.

In Figure 13, we have superposed the power-law relation of the two-point correlation function for rich clusters of galaxies derived by Postman et al. (1992). The amplitude of spatial correlation function for the Tololo grouping is consistent with that of rich clusters.

6.3. *Superclustering of the Absorbers*

The detection of correlation on velocity scales out to 7000 km s^{-1}, or comoving spatial scales of $\sim$30–40 h^{-1} Mpc, is consistent with the result of HHW, who found significant correlations out to velocity separations of 10,000 km s^{-1} corresponding to spatial scales of $\sim 60\ h^{-1}$ Mpc in the SBS sample of C IV systems. We also find evidence for marginally significant spatial clustering on comoving scales of $r < 18\ h^{-1}$ Mpc. Even for the richest clusters of galaxies, $\xi(r) < 1$ on comoving spatial scales less than $\sim 25\ h^{-1}$ Mpc. Our results suggest clustering on scales larger than that of present-day cluster correlations and appear to be consistent with scales characteristic of superclusters.

The stronger clustering amplitude toward the Tololo QSOs as compared with the observed correlations of the richest clusters of galaxies can be viewed in one of two ways: (1) we are viewing only a small region of space where there is a strong departure from the average clustering properties of galaxy clusters; or (2) we are seeing evidence for clustering on supercluster scales. Our data do not sample a sufficient volume of space to distinguish between the two scenarios.

The spatial correlation functions of clusters of galaxies are calculated in volumes considerably larger than our pencil-beam study and, therefore, represent an average $\xi(r)$ over a large volume of space. On the other hand, this work samples only a small fraction of the entire volume, and the correlation signal may represent a region of strong biasing. However, correlations on such large scales are not unprecedented. For example, HHW attribute the clustering signal out to velocities of 10,000 km s^{-1} as being due to a large cluster of systems in the QSO PKS 0237−233. In fact, if PKS 0237−233 is replaced by one of the Tololo QSOs, the correlation amplitude between 1000 and 10,000 km s^{-1} becomes $\xi(v) = 0.26 \pm 0.12$ for Tol 1037−2704 and 0.21 ± 0.12 for Tol 1038−2712 (HHW). Therefore, the clustering signal of the individual lines of sight remains significant even in an average sample of C IV absorbers, although the amplitude is diminished from the value computed using only the four Tololo QSOs.

Bahcall & Burgett (1986) have studied the spatial correlation function of a sample of superclusters from the catalog of Bahcall & Soneira (1984). The sample is complete to $z \leq 0.08$ and contains 16 superclusters with RC ≥ 1 clusters and overdensity factor $f = 20$, and 26 with RC ≥ 0 clusters and $f = 20$. The results of their study reveal correlations at significance levels of 2–3 σ on scales as large as $\sim$75–150 h^{-1} Mpc. Fitting a power law of the form $r^{-1.8}$ which best fits the galaxy and cluster correlation functions, they found

$$\xi_{\rm SC} \simeq \left(\frac{r}{60}\right)^{-1.8}, \qquad (6)$$

with a factor of 2 uncertainty, although it is not obvious that the supercluster correlation function should follow the power-law form. The implied correlation scale of superclusters is $\sim 60\ h^{-1}$ Mpc. Similar results have been obtained by Kopylov et al. (1987), who studied the correlation function out to $z = 0.2$.

Assuming the same power-law form, the peak in the correlation function in Figure 12 implies a correlation scale of $\sim 50\ h^{-1}$ Mpc with an associated uncertainty of $\sim$20%. The supercluster correlation function of Bahcall & Burgett was calculated between spatial scales of $\sim$70–150 h^{-1} Mpc since no meaningful correlation is expected below the typical separation between superclusters ($\gtrsim 60\ h^{-1}$ Mpc). On the other hand in our pencil-beam experiment correlations on scales less than 60 h^{-1} Mpc can be expected because we are likely viewing the linear distances between superclusters in projection and we estimated the correlation scale from a single point at 35 h^{-1} Mpc. Despite the differences between the methods of calculating the correlation functions, we find the characteristic scale of clustering determined from our data to be remarkably consistent with that derived by Bahcall and Burgett for superclusters in the local universe.

7. DISCUSSION

Arguments favoring an intervening supercluster to explain the apparent overdensity of C IV systems in the sight lines to Tol 1037−2704 and Tol 1038−2712 have been presented by S87. They have suggested that in order to get the rich absorption spectra in the two lines of sight, the supercluster must be oriented in such a way that there is an unusually high density of absorbing matter along the lines of sight. The most plausible explanation is that our line of sight coincides with either the long axis of a large-scale "filament" or the plane of a large-scale "sheet" of galaxies. Our results are consistent with, and strengthen the support for, the interpretation of the C IV absorption line systems as arising from material associated with a supercluster.

Our search for C IV absorption line systems in the spectra of the two nearby QSOs, Tol 1035−2737 and Tol 1029−2654, have revealed several new absorption complexes with redshifts coincident to those in the original Tololo pair. In addition to the five matches between the sight lines to Tol 1037−2704 and Tol 1038−2712, at least four of the five complexes in Tol 1035−2737 appear to match systems in Tol 1038−2712, and both complexes in Tol 1029−2654 seem to have redshifts in common with systems in both Tol 1037−2704 and Tol 1038−2712.

As a test of whether the absorbers along the lines of sight to the Tololo QSOs are in any way associated, we evaluated the significance of the apparent correlations in two ways. First, we calculated the probability of obtaining the observed number of matches between adjacent lines of sight, allowing a system in a given line of sight to match at most one system from each of the other lines of sight to within the redshift window Δz. We took Tol 1038−2712 as the fiducial object since the systems in its spectrum match with the most number of systems along the other three lines of sight, noting that in some cases this gives the more optimistic measure of the significance. At the large angular separations of the neighboring QSOs, larger velocity separations can be expected between the C IV systems due to Hubble flow if the expansion of the absorbing structure has a nonperpendicular component to the line of sight, and the redshift window in which possibly correlated absorption can be found is correspondingly larger, increasing the probability of finding spurious absorption matches.

The velocity shift expected from Hubble expansion between absorbers located on two sight lines separated by the perpendicular distance $D_\perp$ and belonging to a comoving structure of

size $R \geq D_\perp$ is given by (J88),

$$\Delta v = H(z) D_\perp \tan \alpha = 2c\theta[(1+z)^{1/2} - 1] \tan \alpha , \quad (7)$$

where $H(z) = H_0(1+z)^{3/2}$ is the value of the Hubble constant at redshift z and $(-\pi/2) \leq \alpha \leq (\pi/2)$ is the angle between the plane of the sky and the line connecting the two absorbers on the two sight lines. If the absorbing material is distributed in a thin sheet then the velocity shifts can be arbitrarily large depending on the orientation of the sheet. For example, for $|\alpha| \simeq \pi/2$ and the sheet is viewed at a glancing angle then the probability of finding spurious absorption systems within the window will be large. For a spherical distribution, however, we have $|\alpha| \leq \pi/4$ and we can evaluate the probability of the detected systems being correlated against the probability of finding similar acceptable redshift coincidences by chance.

For Tol 1037−2704, the velocity separation expected from the Hubble expansion is $\Delta v \simeq 2000$ km s^{-1} or $\Delta z \simeq 0.02$; for Tol 1035−2737, $\Delta v \simeq 5000$ km s^{-1} or $\Delta z \simeq 0.05$; and for Tol 1029−2654, $\Delta v \simeq 20{,}000$ km s^{-1} or $\Delta z \simeq 0.20$. We have organized the C IV absorption systems in Table 9 such that they coincide in velocity to better than that expected from the Hubble flow. In fact, as we can see in Table 9, the systems in Tol 1038−2712 coincide to better than $\Delta v \simeq 4000$ km s^{-1} and 3000 km s^{-1} with those in Tol 1035−2737 and Tol 1029−2654, respectively, so we adopt these values as our criterion for a match. Nevertheless, a few of the pairings are somewhat arbitrary. For example, the $z_{abs} = 1.7306$ system in Tol 1035−2737 could be matched with either the $z_{abs} \simeq 1.755$ or $z_{abs} \simeq 1.777$ systems in Tol 1038−2712. Similarly the $z_{abs} = 1.9852$ system in Tol 1029−2654 could be associated with the

TABLE 9

C IV ABSORPTION LINE MATCHES

Tol 1037-2704	Tol 1038-2712	Tol 1035-2737	Tol 1029-2654
1.48248			
1.48323			
1.63336			
1.63434			
		1.70313	
	1.75530	1.73058	
	1.77688		
	1.77764		
	1.85055	1.84089	
1.91249	1.89309	1.92965	
	1.89353		
1.97145	1.95490		
1.97216	1.95610		
	1.96047		
2.00336			
			2.01744
2.02509			2.01840
2.02785	2.01378		2.02549
2.02847	2.01623		2.02616
2.03915			2.02660
			2.02716
2.07059			
2.07716	2.07660		
2.07858			
2.08321			
2.10663			
2.11561			
2.12818			
2.13593			
2.13910	2.14674	2.12630	
2.14030			
2.14239			

$z_{abs} \simeq 1.972$ and 1.955 systems in Tol 1037−2704 and Tol 1038−2712, respectively, or with the $z_{abs} \simeq 2.003$ system in Tol 1037−2704.

We calculated the significance of the matches in Table 9 by distributing the number of systems observed in each of Tol 1037−2704, Tol 1035−2737 and Tol 1029−2654 over the redshift window in which systems would have been observed in the spectrum of Tol 1038−2712, and evaluating the binomial probability $P(M, N, q)$ that one would obtain the observed number of coincidences N given the number of systems M in the fiducial line of sight, where q is the probability that a system match within Δz of another in the total redshift window Δ. For Tol 1037−2704, $\Delta = 0.73$; for Tol 1035−2737, $\Delta = 0.69$; and for Tol 1029−2654, $\Delta = 0.49$. In this calculation, we counted each complex as one system since members of a complex are not independent, and require that each system in a given spectrum coincide with only one other in the reference spectrum Tol 1038−2712. For Tol 1037−2704, the probability is $P(8, 5, 0.055) \simeq 3 \times 10^{-3}$; for Tol 1035−2737, $P(8, 4, 0.12) \simeq 0.3$; and for Tol 1029−2654, $P(8, 1, 0.082) \simeq 0.6$.

The significance of the absorption matches is high between the original pair, but poor for the other two lines of sight. In fact, if we use Tol 1037−2704 as the fiducial object, the probability of obtaining five matches in Tol 1038−2712 becomes $P \simeq 0.02$, consistent with only a marginal significance for those matches. As pointed out by S87, the high density of absorption systems observed in a narrow redshift range increases the probability that the pattern of redshift matches is due to chance. Moreover, because we have no way of knowing, post hoc, whether we have grouped the systems correctly in Table 9, this calculation is prone to significant uncertainty.

An alternative to the probability calculations above, which does not require a fiducial choice, is to take each absorber in turn and find its closest velocity match in each of the *other* lines of sight. Note that this probability calculation allows for a system to match more than one system in the other lines of sight. The histogram of velocity differences is shown in Figure 14. We also randomly selected absorbers among the four lines of sight for 1000 realizations, preserving the number of absorbers along each sight line and found their closest velocity match. By using these distributions of δv (observed and simulated), we obtained some idea about the significance of the observed matches.

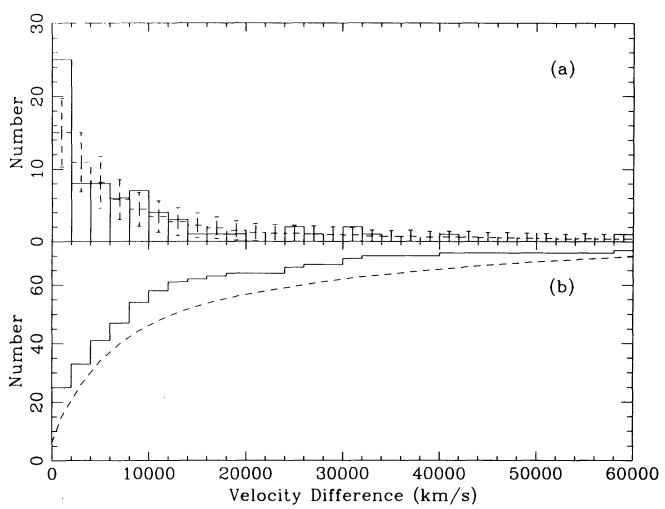

FIG. 14.—(*a*) Distribution of velocity differences between "nearest neighbors" in different lines of sight for the observed (*solid histogram*) and simulated (*dashed histogram*) systems. (*b*) Cumulative distribution of velocity differences for the observed (*solid line*) and simulated (*dashed line*) systems.

The simulated distribution (*dashed histogram*) and its standard deviation (*error bars*) are shown in Figure 14*a*. For velocity differences $\Delta v \leq 2000$ km s^{-1} the observed distribution deviates from randomly distributed redshifts at the $\sim 2.1\ \sigma$ level. In Figure 14*b*, we have plotted the cumulative distributions for the simulated and observed redshifts. A KS test gives a $\sim 1.7\%$ probability that the observed redshifts are drawn from a random population of redshifts, indicating that the correlation between the C IV systems among all four lines of sight is marginal. This agrees with the above probability analysis, which showed weak evidence for correlations between pairs of sight lines.

There is clearly an overdensity of C IV absorbers toward Tol 1037−2704 and Tol 1038−2712. Indeed, that is what first called attention to these QSOs. We can estimate the overdensity of these systems from the average background number density of systems per unit redshift given in Steidel (1990). Over the redshifts spanned by our data, the mean number density of systems per unit redshift interval taken from Steidel (1990) is $dN/dz \sim 2.8$ for systems with rest equivalent widths $W_0 > 0.15$ Å, leading to an expected number of C IV doublets of ~ 2 in Tol 1037−2704 and ~ 2.5 in Tol 1038−2712, over the path lengths searched for C IV absorption. The observed number of detections is 12 in Tol 1037−2704 and 5 in Tol 1038−2712 for the same equivalent width limit. This represents a factor of ~ 6 overdensity in Tol 1037−2704 and ~ 2 in Tol 1038−2712.

We can also estimate the overdensity of C IV absorption systems along the lines of sight to Tol 1035−2737 and Tol 1029−2654. Taking the mean number density of systems again from Steidel (1990) and restricting the wavelength range to the region from Lyman-α to long wavelength limit of the spectrum, 4360–5130 Å, we predict the number of systems with $W_0 > 0.15$ Å to be ~ 1.5 with $W_0 > 0.15$. We observe 2 C IV absorption systems in each of Tol 1035−2737 and Tol 1029−2654 that meet the same equivalent width criterion, evidence of no overdensity in C IV absorbers. However, this calculation ignores the fact that most of the C IV systems observed in Tol 1035−2737 and Tol 1029−2654 lie in the narrow redshift range in which we observe coincidences. Restricting the redshift range to the region exhibiting coincident C IV systems, the predicted number of systems is ~ 1 in each spectrum. The observed number of detections in Tol 1029−2654 over this redshift range could be taken as offering marginal evidence for a factor of 2 overdensity. Finally, we note that the number of detections represent lower limits since the spectra are not sensitive to systems with $W_0 > 0.15$ over their entire wavelength range.

The spatial overdensity of intervening clouds toward the Tololo QSOs lend further support for the interpretation that the four lines of sight intersect material associated with an intervening supercluster. The presence of an overdensity in the spectrum of the most distant QSO Tol 1029−2654 in the group suggests a lower limit on the size of the supercluster of $\sim 30\ h^{-1}$ Mpc in the transverse direction. Taking only the redshift range ($1.73 \leq z \leq 2.15$) in which we observe coincident systems, we estimate the proper linear extent along the line of sight to be $\sim 80\ h^{-1}$ Mpc.

Structures of this size are observed in the local universe. Typical superclusters have dimensions anywhere from 30–150 h^{-1} Mpc for the highest to lowest density systems (Bahcall & Soneira 1984). In addition, studies of the spatial distribution of

rich clusters show evidence for superclustering on scales of ~ 50–$150\ h^{-1}$ Mpc (Bahcall & Soneira 1983, 1984; Postman et al. 1992). There is also considerable evidence from surveys of the local galaxy distribution for large coherent structures extending over many tens of Mpc (see, e.g., de Lapparent, Geller & Huchra 1986). The dimensions of the largest known structure, "The Great Wall," are at least $\sim 60 \times 170\ h^{-1}$ Mpc (Geller & Huchra 1989). If large-scale structures participate in the general Hubble flow, then the dimensions of the observed intervening matter are more like $\sim 90 \times 240\ h^{-1}$ Mpc and the most likely local counterparts are structures such as the "Great Wall."

Recent $\Omega = 1$ cold + hot dark matter (CHDM) N-body simulations, which probe scales of $\sim 50\ h^{-1}$ Mpc, find coherent large scale structures composed of massive galaxy halos to be already in place at $z \sim 2$ (Primack 1995). Smaller scale CDM simulations, which incorporate hydrodynamics and form galaxies over a range of masses, predict $\xi(r) < 1$ on comoving scales of $10\ h^{-1}$ Mpc at $z \sim 2$ (Evrard et al. 1994). In all hierarchical clustering models, the amplitude of large structures is lower at $z \sim 2$ than observed in the local universe. Whether or not the large clustering amplitude seen along the lines of sight toward the Tololo QSOs is in conflict with the standard CDM model depends on what type of galaxy halo is represented by the C IV absorbers. In this paper, we have focused on a region known to have an overdensity of absorbers. If strong clustering signals are seen along other lines of sight, they could pose a considerable challenge to theories of large-scale structure formation.

A remaining complication with the supercluster hypothesis is the presence of the smooth, broad C IV system at $z_{abs} \simeq 2.08$ in Tol 1038−2712, which is not resolved into individual C IV doublets even at the resolution of our data. Such systems are most commonly associated with BAL QSOs. An alternative explanation that is consistent with the intervening supercluster hypothesis is if the line of sight to Tol 1038−2712 pierces a cooling flow associated with the cores of clusters and groups of galaxies. The FWHM of the each component of the C IV absorption doublet at $z_{abs} \simeq 2.08$ is ~ 13 Å, corresponding to a velocity spread of ~ 800 km s^{-1}. The expected velocity range from a single cooling flow seen in absorption is expected to be comparable to the line widths of the emission-line nebulae, or ~ 500–1000 km s^{-1} (Baum 1992). Since all our knowledge of cooling flows comes from low-redshift clusters, it is yet to be determined whether the properties of high-redshift cooling flows are consistent with what we observe in Tol 1038−2712. Crawford et al. (1987) argue that the covering factor is sufficient for *most* lines of sight to pass through a cooling flow, though their estimate of the cooling radius may be overestimated by factors of ~ 2–10.

Further mapping of the large-scale distribution of the intervening absorption clouds toward the Tololo QSOs clearly requires a larger grid of absorption probes. The multiplex advantage of multifiber spectrographs offers a promising and efficient means of sampling many QSOs (>40 in a 2 deg^2 field) simultaneously with sufficient S/N to be sensitive to C IV absorption. Studies of this kind will provide important information on the growth and evolution of large-scale structure in the early universe.

We acknowledge useful conversations with Craig Foltz, Craig Hogan, Ray Weymann, Julia Indik, and Gerry Williger, and excellent support from the technical staff at CTIO. We are grateful to Jill Bechtold and Tom Aldcroft for making their spectral analysis software available to us. This research was supported by NSF grants AST 90-01181 and 93-20715.

REFERENCES

Aaronson, M., McKee, C. F., & Weisheit, J. C. 1975, ApJ, 198, 13
Bahcall, J. N. 1968, ApJ, 153, 679
Bahcall, N. A., & Burgett, W. S. 1986, ApJ, 300, L35
Bahcall, N. A., & Soneira, R. M. 1983, ApJ, 270, 20
———. 1984, ApJ, 277, 27
Baum, S. A. 1992, in Proc. NATO Advanced Study Institute, Clusters and Superclusters, ed. A.C. Fabian (Dordrecht: Kluwer), 171
Bechtold, J. 1994, ApJS, 91, 1
Bergeron, J., & Boisse, P. 1991, A&A, 243, 344
Blades, J. C. 1988, in QSO Absorption Lines: Probing the Universe, ed. J. C. Blades, D. A. Turnshek, & C. A. Norman (Cambridge: Cambridge Univ. Press), 147
Bohuski, T. J., & Weedman, D. W. 1979, ApJ, 231, 653
Broadhurst, T. J., Ellis, R. S., Koo, D. C., & Szalay, A. S. 1990, Nature, 343, 726
Christiani, S., Danziger, I. J., & Shaver, P. A. 1987, MNRAS, 227, 639
Crawford, C. S., Crehan, D. A., Fabian, A. C., & Johnstone, R. M. 1987, MNRAS, 224, 1007
Crotts, A. P. S. 1985, ApJ, 298, 732
Davis, M., & Peebles, P. J. E. 1983, ApJ, 267, 465
de Lapparent, V., Geller, M. J., & Huchra, J. P. 1986, ApJ, 302, L1
Evrard, A. E., Summers, F. J., & Davis, M. 1994, ApJ, 422, 11
Foltz, C. B., Weymann, R. J., Morris, S. L., & Turnshek, D. A. 1987, ApJ, 317, 450
Foltz, C. B., Weymann, R. J., Peterson, B. M., Sun, L., Malkan, M. A., & Chaffee, F. H. 1986, ApJ, 307, 504
Foltz, C. B., Hewett, P. C., Chaffee, F. H., & Hogan, C. J. 1993, AJ, 105, 22
Francis, P. J., & Hewett, P. C. 1995, AJ, 105, 1633
Geller, M. J., & Huchra, J. P. 1989, Science, 246, 897
Heisler, J., Hogan, C. J., & White, S. D. M. 1989, ApJ, 347, 52 (HHW)
Horne, K. 1986, PASP, 96, 609
Jakobsen, P., Perryman, M. A. C., & Cristiani, S. 1988, ApJ, 326, 710 (J88)
Jakobsen, P., & Perryman, M. A. C. 1992, ApJ, 392, 432 (J92)
Jakobsen, P., Perryman, M. A. C., Ulrich, M. H., Macchetto, F., & Di Serego Alighieri, S. 1986, ApJ, 303, L27 (J86)
Kaiser, N., & Peacock, J. A. 1991, ApJ, 379, 482
Kopylov, A. I., Kuznetsov, D. Yu., Fetisova, T. S., & Shvartsman, V. F. 1987, in Proc. Semin. Large-Scale Structure of the Universe (Stavropol: Spec. Astrophys. Obs.), 39
Morton, D. C., York, D. G., & Jenkins, E. B. 1988, ApJS, 68, 449
Olivier, S. S., Primack, J. R., Blumenthal, G. R., & Dekel, A. 1993, ApJ, 408, 17
Postman, M., Huchra, J. P., & Geller, M. J. 1992, ApJ, 384, 404
Primack, J. R. 1995, private communication
Robertson, J. G. 1987, MNRAS, 227, 653
Romani, R. W., Filippenko, A. V., & Steidel, C. C. 1991, PASP, 103, 154
Sargent, W. L. W., Boksenberg, A., & Steidel, C. C. 1988, ApJS, 68, 539 (SBS)
Sargent, W. L. W., & Steidel, C. C. 1987, ApJ, 322, 142 (S87)
Steidel, C. C. 1990, ApJS, 72, 1
———. 1993, in The Evolution of Galaxies and Their Environment, ed. J. M. Shull & H. Thronson (Dordrecht: Kluwer), 263
Weymann, R. J., Carswell, R. F., & Smith, M. G. 1981, ARA&A, 19, 41
Young, P. J., Sargent, W. L. W., & Boksenberg, A. 1982, ApJ, 252, 10
Young, P. J., Sargent, W. L. W., Boksenberg, A., Carswell, R. F., & Whelan, J. A. J. 1979, ApJ, 229, 891
Zabludoff, A. I., Geller, M. J., Huchra, J. P., & Vogeley, M. S. 1993, AJ, 106, 1273